https://doi.org/10.5194/egusphere-2026-4221
Preprint. Discussion started: 17 July 2026
© Author(s) 2026. CC BY 4.0 License.

Contrasting drivers of riparian–stream hydrological dynamics during rainfall events across forest headwater ecoregions

José L. J. Ledesma[1,2], Paul D. Burkhardt[2], Susana Bernal[3], and Andreas Musolff[2]

[1]Department of Biogeochemistry and Microbial Ecology, National Museum of Natural Sciences – Spanish National Research Council (MNCN-CSIC), Madrid, 28006, Spain
[2]Department of Hydrogeology, Helmholtz Centre for Environmental Research (UFZ), Leipzig, 04318, Germany
[3]Integrative Freshwater Ecology Group, Centre for Advanced Studies of Blanes – Spanish National Research Council (CEAB-CSIC), Blanes, 17300, Spain

Correspondence to: José L. J. Ledesma (jose.ledesma@mncn.csic.es)

Abstract. Examining how hydrological responses of streams and riparian groundwater interact during rainfall events can help understand runoff generation mechanisms and their links to biogeochemistry. We analysed rainfall–runoff events in four forest headwater catchments spanning semiarid Mediterranean, subhumid Mediterranean, temperate, and boreal ecoregions. Using sub-daily data, we evaluated how hydroclimatic drivers shaped stream and riparian groundwater. We additionally focussed on the slope (*slopeLin*) and hysteresis (*h*) of the riparian groundwater–stream relationship, describing coupled responses and connectivity patterns. Rainfall amount and antecedent wetness primarily controlled individual stream and riparian groundwater hydrological response across sites, while the vertical activation of riparian layers, defined by *slopeLin*, and timing, defined by *h*, were site-specific. At the Mediterranean sites, deep, low-conductivity layers dominated the lateral connectivity unless sufficient rainfall and wetness allowed activation of shallower flow pathways. At the temperate and boreal sites, shallow, conductive layers were typically active, with temporary disconnection during warm periods at the temperate site and snowmelt-induced activation of upslope sources at the boreal. Clockwise hysteresis, indicating faster riparian than stream responses, prevailed at the temperate and boreal sites. The Mediterranean sites showed weaker or anticlockwise patterns, suggesting activation of other water sources, likely ephemeral tributaries during intense rainfall. Our results show that the activation and hysteresis of riparian–stream connectivity differs across ecoregions, which has implications for solute mobilization. This framework provides a physically grounded perspective for interpreting both rainfall–runoff and concentration–discharge relationships, which can help predict shifts in catchment functioning under changing hydroclimatic regimes.

1 Introduction

Studying hydrological responses to rainfall events at the catchment scale is fundamental to understanding runoff generation mechanisms (Botter et al., 2013; Blöschl et al., 2019). Exploring the drivers of these responses can therefore provide

https://doi.org/10.5194/egusphere-2026-4221
Preprint. Discussion started: 17 July 2026
© Author(s) 2026. CC BY 4.0 License.

valuable insights into catchment hydrological dynamics, improving the reliability of hydrological models and supporting evidence-based management of river networks (Beven, 2019).

In non-alpine, forest headwater catchments, typically characterized by moderate relief and simple drainage networks, hydroclimatic variables often emerge as key drivers of rainfall–runoff responses. While catchment typology (land use, vegetation, and geology), topography (terrain slope), and topology (drainage network configuration) are widely recognized as foundational controls on runoff generation under given climatic settings (Buttle, 2006), hydroclimatic factors such as rainfall characteristics or antecedent conditions may exert a more immediate influence. Although numerous studies have explored those relationships within individual regions (e.g., Hövel et al., 2025), cross-ecoregional comparisons remain relatively rare (e.g., Ali et al., 2015). Such comparisons offer valuable opportunities to identify both common and contrasting responses and their drivers across different environmental contexts.

Any given hydrological response is undoubtedly linked to rainfall amount. However, rainfall intensity can be even more influential, particularly in drier environments, as it can trigger the development of hydrological connectivity through non-linear threshold responses (Gomi et al., 2008; Azarnivand et al., 2020; Ledesma et al., 2021a). Soil moisture conditions, especially those preceding rainfall events, have also been identified as key drivers of hydrological responses (Penna et al., 2011; Singh et al., 2021; Hövel et al., 2025). In general, drier antecedent conditions result in weaker responses, owing to low hydrological connectivity within the catchment. Because soil moisture measurements are not always available, proxies such as antecedent precipitation and runoff coefficient (RC) are often used for the catchment's antecedent wetness state and hydrological efficiency, respectively (e.g., Hughes and Metzler, 1998; Ledesma et al., 2022). Seasonality, largely represented by potential evapotranspiration (PET) integrating seasonal cycles of temperature and vegetation, can also influence hydrological responses by shaping patterns of water availability and storage (Carey et al., 2010). Integrated aridity metrics, such as the dryness index (DI, as PET divided by precipitation) are also commonly used, as they combine seasonal and wetness-related influences to characterize hydrological constraints (Tarasova et al., 2018). Collectively, all these factors and their interactions can shape hydrological responses in diverse ways (Knapp et al., 2025), with effects that may vary depending on each catchment's environmental context, an aspect that remains underexplored in the literature.

Hydrological responses to rainfall events are reflected not only in stream discharge but also in interdependent changes in groundwater table. This is particularly relevant within near-stream riparian zones that play a key role in runoff generation (McGlynn and McDonnell, 2003; Martínez-Carreras et al., 2015). Relationships between stream discharge and riparian groundwater table, specifically hysteresis patterns, can provide valuable insights into rainfall–runoff dynamics and support a more integrated understanding of catchment hydrological response (Gelmini et al., 2022). This relationship often exhibits a clockwise pattern, with riparian groundwater table higher during the rising than the falling limb of the hydrograph, indicating that the riparian zone responds more rapidly and feeds the stream (Jung et al., 2004; Frei et al., 2010; Fovet et al., 2015). Yet, anticlockwise patterns have also been observed under very wet antecedent conditions, suggesting widespread hydrological connectivity across the catchment beyond the riparian zone (Ledesma et al., 2022). Investigating these hysteresis relationships is valuable because solute mobilization from catchments predominantly depends on which riparian soil layers

https://doi.org/10.5194/egusphere-2026-4221
Preprint. Discussion started: 17 July 2026
© Author(s) 2026. CC BY 4.0 License.

become hydrologically connected to the stream, and when. Because solute concentrations in riparian zones often vary with depth (Stewart et al., 2022; Ledesma et al., 2025), the timing and sequence of connectivity, or lack thereof, are critical for interpreting biogeochemical responses during rainfall–runoff events.

In this study, we analysed more than 200 rainfall–runoff events in four non-alpine, forest headwater catchments spanning distinct ecoregions: semiarid Mediterranean, subhumid Mediterranean, temperate, and boreal. We evaluated the role of potential hydroclimatic drivers, including rainfall event characteristics and antecedent catchment wetness (using precipitation), seasonality (using PET), aridity (using DI), and hydrological efficiency (using RC), in shaping hydrological responses. These responses include variations in stream discharge and riparian groundwater table, as well as the dynamic relationship between them, with particular attention to slope and hysteresis patterns of that relationship. Our ultimate aim was to identify both shared and ecoregion-specific hydrological responses and their drivers across diverse environmental settings. This knowledge can contribute to a more integrated understanding and improved management of river networks and their hydrological functioning under environmental change.

2 Materials and Methods

Throughout the manuscript, we refer to “rainfall” when describing specific hydrometeorological episodes that triggered discharge responses (i.e., rainfall–runoff events) and their characteristics, and to “precipitation” when calculating antecedent conditions or more broadly when referring to water input over longer time scales.

2.1 Characterization of study sites

The two Mediterranean sites are headwaters of the 865 km² Tordera catchment in north-eastern Spain, which drains into the Mediterranean Sea. The Tordera spans a wide elevation range, creating diverse orographic and climatic conditions that support varied hydrological regimes including perennial, intermittent, and ephemeral streams. *Fuirosos* (16.5 km^2) is located in the Montnegre Corredor range (Fig. 1a), with mild winters, wet springs and dry summers, typically semi-arid Mediterranean due to the high evapotranspiration in relation to the precipitation. Mean annual temperature and precipitation (2009-2023) are 14.2 °C and 645 mm, respectively. *Font del Regàs* (15.5 km^2) lies in the Montseny massif (Fig. 1b), with a seasonality of temperature and precipitation similar to that of *Fuirosos*, but overall cooler and wetter climate, defined as subhumid Mediterranean. Mean annual temperature and precipitation (2009-2023) are 11.3 °C and 933 mm, respectively. At both sites, evergreen species of trees including oak and pine dominate the forest landscape, with large proportions of deciduous beech present in upper parts of the subhumid site. Riparian forest dominates the near-stream areas of the lower parts of both catchments, including species of alder, poplar, and plane. The bedrock in the region is granitic and soils at both sites are predominantly sandy (Bernal et al., 2002; Lupon et al., 2016).

The 520 km^2 Rappbode Reservoir system is located in the Harz Mountains of Central Germany and provides drinking water to more than one million people (Wollschläger et al., 2017). The 2.58 km^2 *Upper Rappbode* experimental catchment (Fig.

https://doi.org/10.5194/egusphere-2026-4221
Preprint. Discussion started: 17 July 2026
© Author(s) 2026. CC BY 4.0 License.

1c) belongs to this reservoir system and has been intensively studied as part of the TERENO observatory (Wollschläger et al., 2017). Mean annual temperature during the last seven years (2018-2024) was 8.0 °C and long-term (1986-2015) mean annual precipitation is 1061 mm (Musolff et al., 2021). Prior to 2018, the landscape was dominated by forest (78%), predominantly spruce, with lower proportions of other vegetation (22%), particularly species of grass present in the riparian zone. The catchment was affected by a multi-year Europe-wide drought starting in 2018, which led to a severe bark beetle infestation and the removal of most of the upslope spruce trees by the end of 2022 (Kong et al., 2022; Musolff et al., 2024; Rakovec et al., 2022). The consequent decrease in evapotranspiration and loss of canopy interception resulted in increased hydrological efficiency in this catchment (Musolff et al., 2024). The underlying bedrock consists of Palaeozoic rocks including greywacke, shale, and diabase (Wollschläger et al., 2017). The upslope soils are mainly cambisols, while riparian zone soils are humic and stagnic gleysols.

The 121 km^2 Krycklan catchment drains into the larger Vindeln river in northern Sweden. The upper 68 km^2 make up the extensively investigated *Krycklan Catchment Study* (KCS), an infrastructure for research in the boreal landscape (Laudon et al., 2021). The climate is subarctic with long-term (1981-2022) mean annual temperature and precipitation of 2.1 °C and 638 mm, respectively. The upper and central parts of the KCS, located above the postglacial coastline, are dominated by coniferous forest stands and patches of wetlands, with occasional deciduous birch in riparian zones. The bedrock is gneissic and Quaternary deposits of glacial till underlie the podzols present in upslopes and the histosols present in the riparian zones.

The four study sites span a broad range of hydroclimatic conditions consistent with the Budyko framework (Ledesma et al., 2025), which relates long-term water and energy availability to dominant catchment water partitioning between evapotranspiration and runoff. In this framework, evapotranspiration dominates in water-limited catchments, whereas runoff dominates in energy-limited catchments. The semiarid Mediterranean site is the driest, with the lowest water yield and signs of evapotranspiration limited by water availability. The temperate site is the most humid, with the highest water yield and a climate typical of energy-limited systems; the boreal site shares this characterization but with less precipitation. The subhumid Mediterranean site lies between the boreal and semiarid sites, near the transition from energy- to water-limited conditions. These climatic differences result in distinct stream discharge patterns. Ledesma et al. (2025) reported the temperate site showing the highest median daily discharge (0.79 mm), followed by the boreal site (0.24 mm), the subhumid site (0.20 mm), and the semiarid site (0.04 mm). The Mediterranean sites exhibit greater hydrological extremes, including both intense storm-driven discharge events and, in the case of the semiarid site, prolonged dry periods typical of intermittent streams.

https://doi.org/10.5194/egusphere-2026-4221
Preprint. Discussion started: 17 July 2026
© Author(s) 2026. CC BY 4.0 License.

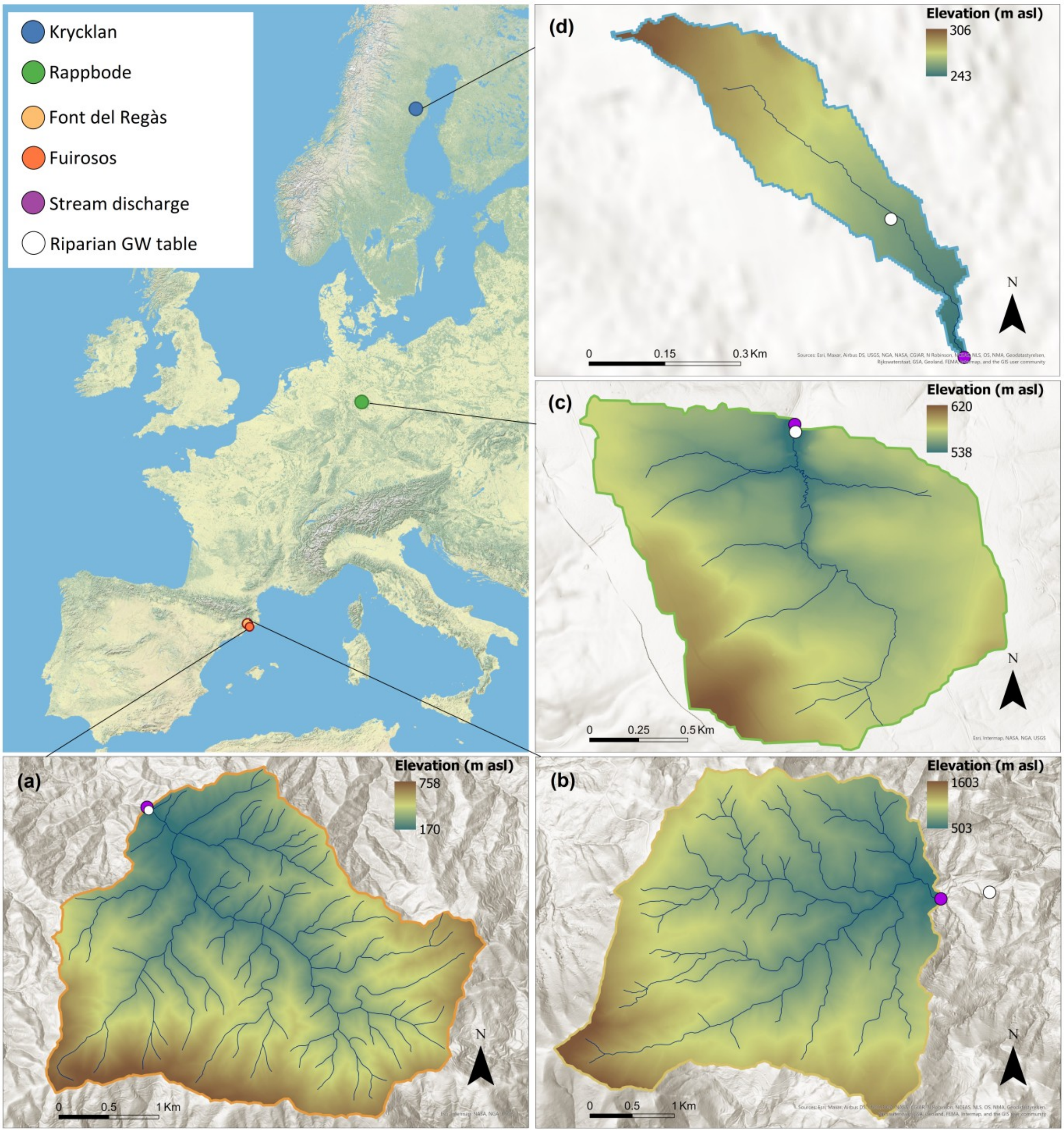

Figure 1: Location of study sites within Europe and catchment delineations at the stations where we measured stream discharge for (a) the semiarid Mediterranean *Fuirosos*, (b) the subhumid Mediterranean *Font del Regàs*, (c) the temperate *Upper Rappbode*, and (d) the boreal *Krycklan C2*. Map sources: Esri, Intermap, NASA, NGA, USGS, Maxar, Airbus DS, CGIAR, N. Robinson, NCEAS, NLS, OS, NMA, Geodatastyrelsen, Rijkswaterstaat, GSA, Geoland, FEMA, and the GIS user community | Powered by Esri.

https://doi.org/10.5194/egusphere-2026-4221
Preprint. Discussion started: 17 July 2026
© Author(s) 2026. CC BY 4.0 License.

2.2 Monitoring data and instrumentation

The core of this study consists of high-frequency data on precipitation, stream discharge, and riparian groundwater table. The monitoring periods varied across variables and sites, with temporal resolution ranging from 10 min to 1 h (Table 1).

Table 1: Data availability at the study sites.

Data	Description	*Fuirosos* (Semiarid Mediterranean)	*Font del Regàs* (Subhumid Mediterranean)	*Upper Rappbode* (Temperate)	*Krycklan C2* (Boreal)
Precipitation	Frequency	30-min	30-min	30-min	10-min
	Period	11/04/2014-11/03/2024	17/04/2014-11/03/2024	26/06/2013-05/02/2025	10/05/2008-15/10/2009
	Missing data	0%	0%	24%	40%
Stream discharge	Frequency	10-min	10-min	15-min	30-min
	Period	11/10/2018-11/03/2024	13/01/2020-11/03/2024	21/05/2013-11/12/2024	06/04/2005-03/09/2024
	Missing data	22%	11%	7%	17%
Riparian groundwater table	Frequency	10-min	10-min	15-min	1-h
	Period	31/10/2019-11/03/2024	17/09/2018-11/03/2024	04/11/2020-22/09/2022	18/05/2008-20/09/2009
	Missing data	34%	11%	24%	2%

At the Mediterranean sites, precipitation data were available from two meteorological stations managed by the Catalan Meteorological Service. *Dosrius* is located ca. 15 km southwest of the outlet of the semiarid *Fuirosos* site, while *Viladrau* station is ca. 4 km northwest of the outlet of the subhumid *Font del Regàs* site. The representativeness of the meteorological data from these two stations was previously assessed and considered descriptive for both catchments (Ledesma et al., 2021a). At the semiarid site, stream discharge was measured at a station draining the upper 9.9 km^2 of the catchment at 41° 43’ N, 2° 34’ E (Fig. 1a). Riparian groundwater table was measured using a HOBO water level data logger at a perforated monitoring well placed at the edge of the stream at this location. At the subhumid site, the stream discharge monitoring station drained the upper 13.0 km^2 of the catchment at 41º 49’ N, 2º 27’ E (Fig. 1b). A perforated monitoring well equipped with a HOBO for riparian groundwater table measurements was 3 m from the stream at a location a few hundred meters downstream, where the drainage area is 14.2 km^2.

At the temperate *Upper Rappbode* site, precipitation data were available from a meteorological station located 350 m from the outlet of the catchment at 51° 39’ N, 10° 42’ E (i.e., at 2.58 km^2), where stream discharge was regularly monitored (Fig. 1c). A few meters upstream, a perforated monitoring well located 10 m from the east-side of the stream was used to record riparian groundwater table. The well was equipped with a Solinst Levelogger pressure transducer.

At the boreal *Krycklan* site, precipitation data were available from the Svartberget field station located at the centre of KCS. Stream discharge was monitored at the subcatchment Västrabäcken, known as *C2*, which drains a small, 100% forest area of 0.12 km^2 at 64° 15’ N, 19° 46’ E (Fig. 1d). A few hundred meters upstream, a perforated monitoring well equipped with a TruTrack water level data logger was used to record riparian groundwater table. The well was placed 4 m from the stream.

https://doi.org/10.5194/egusphere-2026-4221
Preprint. Discussion started: 17 July 2026
© Author(s) 2026. CC BY 4.0 License.

For this study, we selected a single monitoring well at each site in the near-stream zone to represent riparian groundwater dynamics and their relationship with stream discharge. This approach is supported by Beiter et al. (2020), who showed that a single well can reliably capture such relationships. To further validate this choice at our sites, we conducted cross-correlation analyses with data from adjacent wells to assess the spatial consistency of riparian groundwater responses. The results revealed no systematic differences in hydrological behaviour across wells (Fig. A1).

2.3 Rainfall–runoff event identification

The time resolution used for rainfall–runoff event identification at each site was determined by the coarsest resolution among precipitation, stream discharge, and riparian groundwater table data (Table 1). Datasets with finer resolutions were aggregated to match this common resolution. As a result, a 30-min resolution was used for both Mediterranean sites and the temperate site, while a 1-h resolution was applied at the boreal site. We only included periods where all three variables were simultaneously available, which resulted in effective monitoring periods ranging from 1 to 4 years, depending on the site.

To focus on rainfall-driven events, we excluded periods influenced by snowfall, rainfall on snow, or snowmelt, typical of the boreal site and, to a lesser extent, the temperate site. These periods were identified and removed based on persistently sub-zero air temperatures and subsequent peaks in stream discharge, which were easily recognizable through visual inspection of temperature records and hydrographs. This exclusion means that we did not attempt to capture the full annual hydrological cycle, but rather focussed specifically on the dynamics of runoff generation during rainfall events, consistent with the study's aim of understanding how these events, and their associated hydroclimatic conditions, influence stream and riparian responses. We note that although snow-related periods were excluded when defining events, some rainfall events that occurred after snowmelt windows may still reflect antecedent conditions influenced by snow. This is particularly relevant for hydroclimatic predictors calculated over 30- or 90-day antecedent periods (Table 2). We argue that such influence is part of the hydrological context shaping rainfall responses and was therefore retained.

Rainfall–runoff events were identified based on changes in stream discharge associated with rainfall of at least 1 mm, using a set of threshold-based criteria. As such, rainfall episodes that did not trigger a sufficient stream response were not considered events and are not part of the dataset. This particularly applies to the semiarid Mediterranean site, where summer rainfall generally failed to generate hydrological responses due to stream intermittency. The beginning of an event (t_0) was defined as the time step immediately preceding a discharge increase of at least 5% (Mediterranean sites), 3% (temperate site), or 10% (boreal site) relative to the previous value. This initial increase had to be followed by a cumulative discharge rise of at least 15% (Mediterranean sites), 10% (temperate site), or 20% (boreal site) over the subsequent 3-hour period. These thresholds were calculated using a rolling sum of discharge changes over successive time steps, allowing for the identification of sustained hydrograph rises in response to rainfall.

The end of an event (t_f) was determined along the recession limb of the hydrograph, based on a composite index that summed discharge changes over a single time step, a 3-hour period, and a 6-hour period. An event was considered to end at the time step where this composite index reached a local minimum below -10% (Mediterranean sites), -5% (temperate site),

https://doi.org/10.5194/egusphere-2026-4221
Preprint. Discussion started: 17 July 2026
© Author(s) 2026. CC BY 4.0 License.

or -20% (boreal site), provided that no lower discharge value with an equally or more negative composite index occurred within the subsequent 3-hour window. This ensured that the end point corresponded to a true stabilization in discharge following the event peak.

The methodology was supported by visual inspection (graphical analysis) of precipitation and discharge time series, which informed the selection of site-specific thresholds and allowed for manual adjustment of individual event boundaries. While various methods have been proposed to make rainfall–runoff event identification more objective and automated (e.g., Giani et al., 2022), relying on expert knowledge, graphical inspection, and catchment-specific thresholds remains a solid approach to ensure hydrologically meaningful event delineation (Thiesen et al., 2019).

2.4 Hydroclimatic predictors and hydrological responses

We selected hydroclimatic variables that described the characteristics of each rainfall–runoff event, or that of corresponding antecedent periods, as potential predictors of hydrological responses. We included the following categories: rainfall characteristics, described by amount (*P*), and mean and maximum intensities (*Pi*, *PiMax*); antecedent wetness, described by antecedent precipitation; seasonality (both antecedent and event-based), described by potential evapotranspiration (*PET*); aridity (both antecedent and event-based), described by the dryness index (*DI*); and antecedent hydrological efficiency, described by the antecedent *RC* (Table 2). As descriptors of antecedent conditions, we used 7, 30, and 90-day periods preceding events to capture short-, medium-, and long-term influences. Note that we did not use 7-day antecedent *PET* (*PET07*) due to its high correlation with *PET30*. Moreover, *DI07*, *RC07*, and *RC30* were also excluded, as their values were often derived from periods with very low or no precipitation, making their interpretation difficult and of limited analytical value.

Table 2: List of hydroclimatic variables calculated for each rainfall–runoff event and used as potential predictors of the hydrological response metrics shown in Table 3. Potential evapotranspiration (*PET*) was calculated with the Penman-Monteith equation (Allen et al., 1998) based on available climatic data from the meteorological stations. Note that 7, 30, and 90-day antecedent variables represent short-, medium-, and long-term preceding influences. Note that *PET07*, *DI07*, *RC07*, and *RC30* were not used (details in the text).

Variable	Units	Category	Definition
P	mm	Rainfall characteristic	Total rainfall amount
Pi	mm day^{-1}	Rainfall characteristic	Mean daily rainfall intensity
PiMax	mm h^{-1}	Rainfall characteristic	Maximum hourly rainfall intensity
P07	mm	Antecedent wetness	7-day antecedent precipitation amount
P30	mm	Antecedent wetness	30-day antecedent precipitation amount
P90	mm	Antecedent wetness	90-day antecedent precipitation amount
PET	mm	Seasonality	Potential evapotranspiration
PET30	mm	Antecedent seasonality	30-day antecedent potential evapotranspiration
PET90	mm	Antecedent seasonality	90-day antecedent potential evapotranspiration
DI	-	Aridity	Dryness index: *PET* divided by *P*

https://doi.org/10.5194/egusphere-2026-4221
Preprint. Discussion started: 17 July 2026
© Author(s) 2026. CC BY 4.0 License.

Variable	Units	Category	Definition
DI30	-	Antecedent aridity	30-day antecedent dryness index: *PET30* divided by *P30*
DI90	-	Antecedent aridity	90-day antecedent dryness index: *PET90* divided by *P90*
RC90	%	Antecedent hydrological efficiency	90-day antecedent runoff coefficient: *Q90* divided by *P90*

We described the hydrological responses (Table 3) of all identified events using stream discharge-related metrics including duration (*L*), average (*Qavg*), total (*Qsum*), maximum (*Qmax*), range (*dQ*), and runoff coefficient (*RC*, as Q divided by P). Additionally, we included average (*GWavg*) and range (*dGW*) as riparian groundwater table-related metrics (Table 3). All these metrics were calculated using data between t_0 and t_f.

We calculated three metrics describing the relationship between stream discharge and riparian groundwater table (Table 3). First, we calculated the slope of the linear relationship between these two variables (*slopeLin*, cm mm^{-1}). This metric serves as a proxy for the average rate at which upper riparian layers are hydrologically activated during the event in relation to increments in stream discharge. Higher values indicate that, on average, rainfall more effectively fills the riparian profile vertically relative to the otherwise dominant lateral transmissivity dimension. Thus, a higher *slopeLin* value corresponds to a relatively lower effective hydraulic conductivity of the activated riparian layers, as vertical saturation increases its importance relative to the lateral flow.

Table 3: List of hydrological response metrics calculated for each rainfall–runoff event.

Metric	Units	Category	Definition (more details in the text)
L	days	Stream discharge	Duration
Qavg	mm day^{-1}	Stream discharge	Average daily stream discharge
Qsum	mm	Stream discharge	Total stream discharge
Qmax	mm h^{-1}	Stream discharge	Maximum hourly stream discharge
dQ	mm	Stream discharge	Stream discharge range: maximum value minus the value at t_0
RC	%	Stream discharge	Runoff coefficient: *Qsum* divided by total rainfall amount *P*
GWavg	cm	Riparian groundwater table	Average riparian groundwater table relative to the time series minimum
dGW	cm	Riparian groundwater table	Riparian groundwater table range: maximum value minus the value at t_0
slopeLin	cm mm^{-1}	Q-GW relationship	Slope of the linear relationship between *Q* and *GW*
h	-	Q-GW relationship	Hysteresis index between *Q* and *GW* based on Zuecco et al. (2016)
hAbs	-	Q-GW relationship	Absolute value of *h*

Second, we calculated the hysteresis index between stream discharge and the corresponding riparian groundwater table (*h*) using the method proposed by Zuecco et al. (2016). This index characterizes the direction, shape, and size of the hysteresis loop: $h > 0$ indicates clockwise hysteresis, $h < 0$ indicates anticlockwise hysteresis, and $h \approx 0$ reflects no clear hysteresis or a complex loop. Here, we used a threshold of $|h| < 0.05$ to define negligible hysteresis, following the general guidance of Zuecco et al. (2016) and its application in recent studies (e.g., Gelmini et al., 2022). Accordingly, values of $h \geq 0.05$ were

https://doi.org/10.5194/egusphere-2026-4221
Preprint. Discussion started: 17 July 2026
© Author(s) 2026. CC BY 4.0 License.

classified as clockwise hysteresis, indicating that riparian groundwater table responds faster to rainfall than stream discharge, while values of $h \leq -0.05$ were classified as anticlockwise hysteresis, suggesting the opposite sequence of responses (i.e., stream discharge responds faster to rainfall than riparian groundwater table). While the sign of *h* relative to these thresholds indicates which variable responds first, the index itself is continuous. As such, higher *h* values always indicate a relatively faster groundwater response, and lower *h* values a relatively faster stream response, regardless of whether *h* is positive or negative.

Finally, the size of the hysteresis loop indicates the discrepancy in response timing between stream discharge and riparian groundwater table. High positive h values correspond to a long lag in stream response relative to riparian groundwater (i.e., the groundwater table responds much faster), whereas high negative h values reflect a long lag in riparian groundwater response relative to the stream (i.e., the stream responds much faster). To quantify the magnitude of this discrepancy, we used the absolute value of the hysteresis index (hAbs).

2.5 Statistical analyses

We tested whether hydroclimatic predictors and hydrological responses differed among sites. We used non-parametric Kruskal–Wallis tests to assess differences among groups, followed by Dunn's post hoc tests with joint ranking for pairwise comparisons and p-value adjustment for multiple testing. Non-parametric tests were chosen due to the non-normal distribution and unequal variances commonly observed in event-scale data. The significance level was set at $p < 0.05$. Additionally, we computed Spearman's rank correlations between hydroclimatic predictors and hydrological response metrics for each catchment.

We used multimodel inference (MMI) (Burnham and Anderson, 2002) to explore the potential of hydroclimatic variables (Table 2) to predict hydrological responses (Table 3) to rainfall events for each catchment separately. Models were applied to all response metrics, but we particularly focus our discussion on *slopeLin* and *h*, as metrics combining stream discharge and riparian groundwater table dynamics. Prior to applying the MMI routine, we z-standardized all variables and tested the collinearity of the predictors. We excluded predictors with variance inflation factors greater than 10, as recommended by Montgomery et al. (2012). As a result, no predictors were excluded for the subhumid Mediterranean site, *P90* and *PET30* were excluded from the analysis for the semiarid Mediterranean site, while *PET30* and DI90 were excluded for both the temperate and boreal sites. We then applied the *dredge*() function from the MuMIn R Package (Bartoń, 2025), which, for each response metric, computes linear regression models for all possible combinations of predictors. To avoid overfitting and maintain an appropriate ratio between the number of predictors and sample size, we restricted models to a maximum of three predictors, consistent with standard practice in MMI frameworks (Burnham and Anderson, 2002).

For each response metric and catchment, we ranked models by their Akaike Information Criterion corrected for small sample size (AICc), retaining only those models with ΔAICc ≤ 2 relative to the best model. For each retained model, we computed the explained variance (R^2), indicating explanatory power, and the Akaike weight (w_i), indicating the relative likelihood of the model being the best among the set. For each response metric, we summarized the explanatory power of the retained models using the mean-weighted explained variance (wR^2), calculated as the weighted average of model-specific R^2 values based on w_i. For each predictor within a given response metric and catchment, we derived a weighted-average of its standardized regression coefficients across all retained models based on w_i. This statistic indicates the strength and direction of the predictor-response relationship. Finally, we also used w_i to calculate the mean-weighted partitioned share of explained variance of each predictor within a given response metric and catchment (Hoffman and Schadt, 2016). These analyses were performed in R version 4.4.3.

3 Results

3.1 Rainfall–runoff event characteristics across sites

We identified a total of 38, 89, 50, and 32 rainfall–runoff events for the semiarid Mediterranean, subhumid Mediterranean, temperate, and boreal sites, respectively. The larger number of events at the subhumid site matches its longer monitoring period and the absence of snow influence or summer flow cessation.

The magnitude of the events in terms of *P* was significantly lower at the temperate site compared with the other sites (Fig. 2a), whereas *Pi* and *PiMax* were significantly larger at the Mediterranean sites (Fig. 2b,c). The results showed only small differences in *PET* and *DI* across sites (Fig. 2d,e). Antecedent wetness as *P07*, *P30* (not shown), and *P90* (Fig. 2f) tended to be lower at the semiarid site, whereas antecedent seasonality, as *PET30* (not shown) and *PET90* (Fig. 2g) tended to be lower at the temperate site. Antecedent aridity, as *DI30* (not shown) and *DI90* (Fig. 2h), tended to be higher at the Mediterranean sites. Finally, antecedent hydrological efficiency (*RC90*) was higher at the temperate site, followed by the boreal, subhumid Mediterranean, and semiarid Mediterranean sites (Fig. 2i). Note that the noticeably higher median *RC90* at the temperate site compared to the boreal site did not translate into a statistically different *RC90* distribution between these two sites.

Differences in hydrological response metrics across sites were, in general, more apparent than the differences in hydroclimatic variables. The duration (*L*) was longest at the boreal site, shortest at the subhumid Mediterranean site, and most variable at the semiarid Mediterranean site (Fig. 3a). The stream discharge response, characterized by *Qsum*, *Qmax*, *dQ* (not shown), and *Qavg* (Fig. 3b), generally mirrored the overall stream discharge distributions at the sites: significantly lower at the Mediterranean sites, particularly at the semiarid, and significantly higher at the temperate and boreal sites, with the temperate site tending to show the highest responses. The *RC* (Fig. 3c) and *GWavg* (not shown) responses followed a similar pattern. By contrast, *dGW* showed no clear statistical differences among sites (Fig. 3d). Yet, the Mediterranean sites generally exhibited milder *dGW* responses (lower median) but also greater variability, including some values higher than those at the temperate and boreal sites.

The rate at which upper riparian layers became hydrologically activated during events, as indicated by *slopeLin*, was higher and more variable at the semiarid Mediterranean site, followed by the subhumid Mediterranean site (Fig. 3e). This rate was lower and comparable at the temperate and boreal sites, although the temperate site showed more outliers. Statistical differences in the hysteresis index *h* among sites were only significant for the subhumid Mediterranean site, which showed

https://doi.org/10.5194/egusphere-2026-4221
Preprint. Discussion started: 17 July 2026
© Author(s) 2026. CC BY 4.0 License.

significantly lower values (Fig. 3f). Nevertheless, the frequency distribution of hysteresis types revealed clear dominant patterns: clockwise hysteresis prevailed at the temperate (58% of events) and boreal (59%) sites, no hysteresis dominated at the semiarid site (53%), and anticlockwise patterns were most frequent at the subhumid site (76%) (Fig. B1).

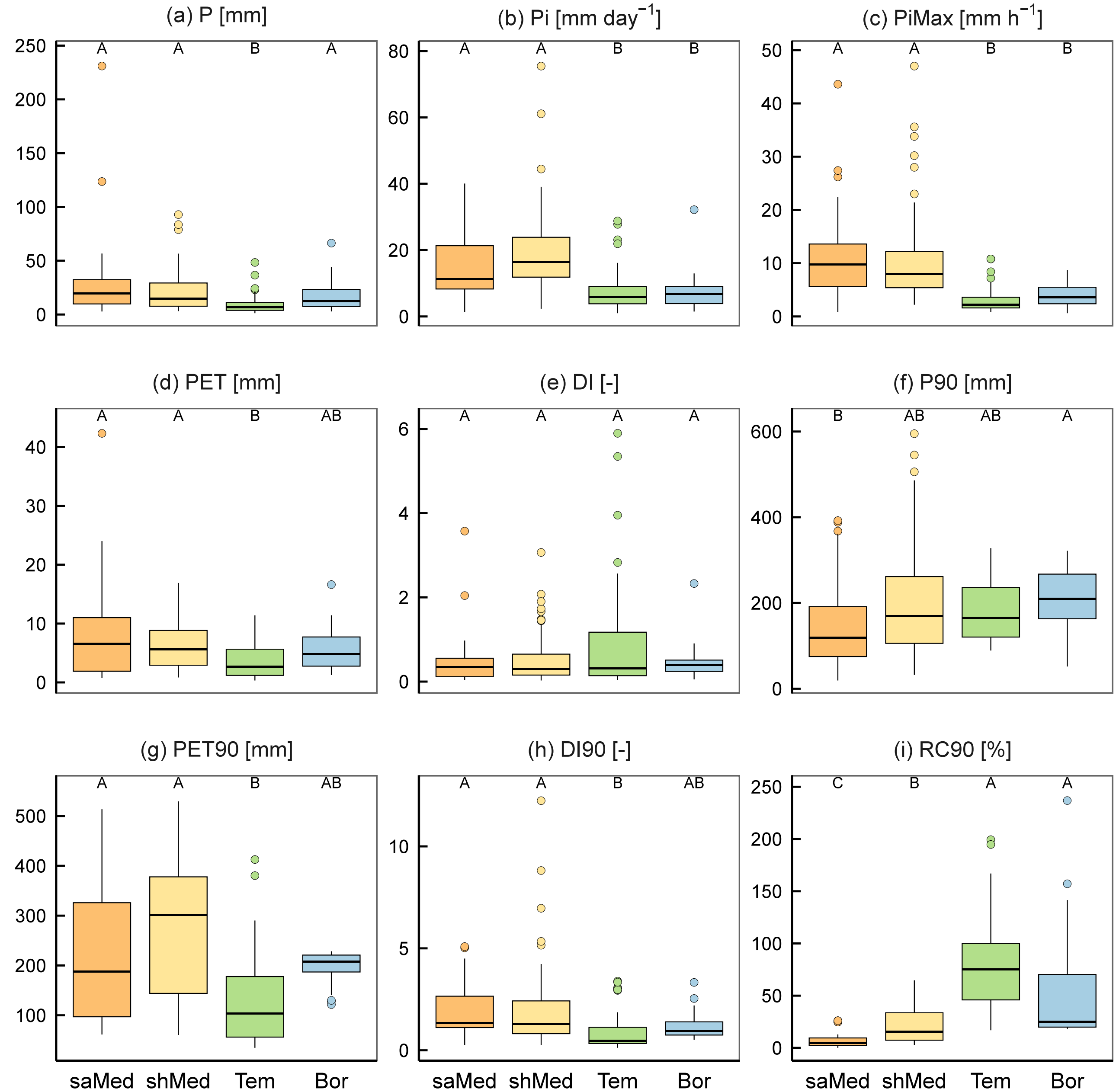

Figure 2: Box plots of selected hydroclimatic variables (Table 2) used as potential predictors of the hydrological response metrics shown in Table 3. Results of Dunn's post hoc tests with joint ranking are indicated by letters; groups not sharing a letter differ significantly at $p < 0.05$. Note saMed: semiarid Mediterranean, shMed: subhumid Mediterranean, Tem: temperate, Bor: boreal.

https://doi.org/10.5194/egusphere-2026-4221
Preprint. Discussion started: 17 July 2026
© Author(s) 2026. CC BY 4.0 License.

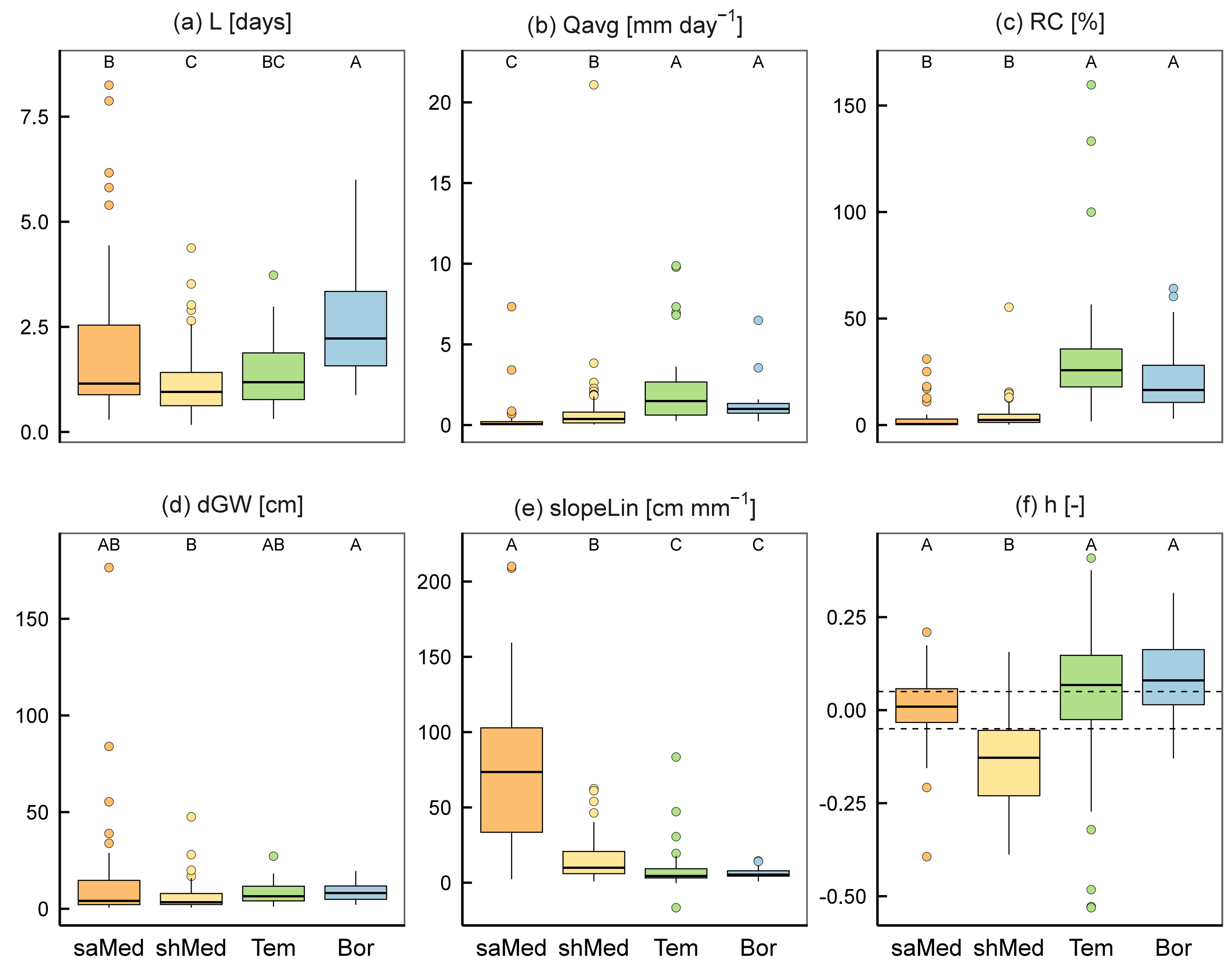

Figure 3: Box plots of selected hydrological response metrics (Table 3). Results of Dunn's post hoc tests with joint ranking are indicated by letters; groups not sharing a letter differ significantly at p < 0.05. In panel (f), dashed lines at ± 0.05 delimit events with negligible hysteresis; values above or below indicate clockwise or anticlockwise hysteresis, respectively. Note saMed: semiarid Mediterranean, shMed: subhumid Mediterranean, Tem: temperate, Bor: boreal.

3.2 Predictor-response relationships during rainfall–runoff events

Spearman's rank correlations between hydroclimatic predictors and hydrological response metrics revealed both similarities and contrasting patterns among sites (Fig. 4). Stream discharge (*L*, *Qavg*, *Qsum*, *Qmax*, *dQ*, *RC*) and riparian groundwater table (*GWavg*, *dGW*) metrics were generally (i) positively correlated with *P* across all sites, and with *Pi* only at the temperate site, (ii) positively correlated with antecedent wetness at the semiarid Mediterranean (especially *P30*), the subhumid Mediterranean (especially *P90*), and the temperate (especially *P07*) sites, but not at the boreal site, (iii) negatively correlated with event-based (*PET*, *DI*) and antecedent seasonality (*PET30*, *PET90*) and aridity (*DI30*, *DI90*) at the temperate site, but

https://doi.org/10.5194/egusphere-2026-4221
Preprint. Discussion started: 17 July 2026
© Author(s) 2026. CC BY 4.0 License.

only with *DI30* and *DI90* at the Mediterranean sites, and (iv) positively correlated with antecedent hydrological efficiency (*RC90*) only at the Mediterranean sites. The Q-GW relationship metrics (*slopeLin*, *h*, *hAbs*) generally showed weaker correlations with hydroclimatic predictors and were explored in more detail using MMI results.

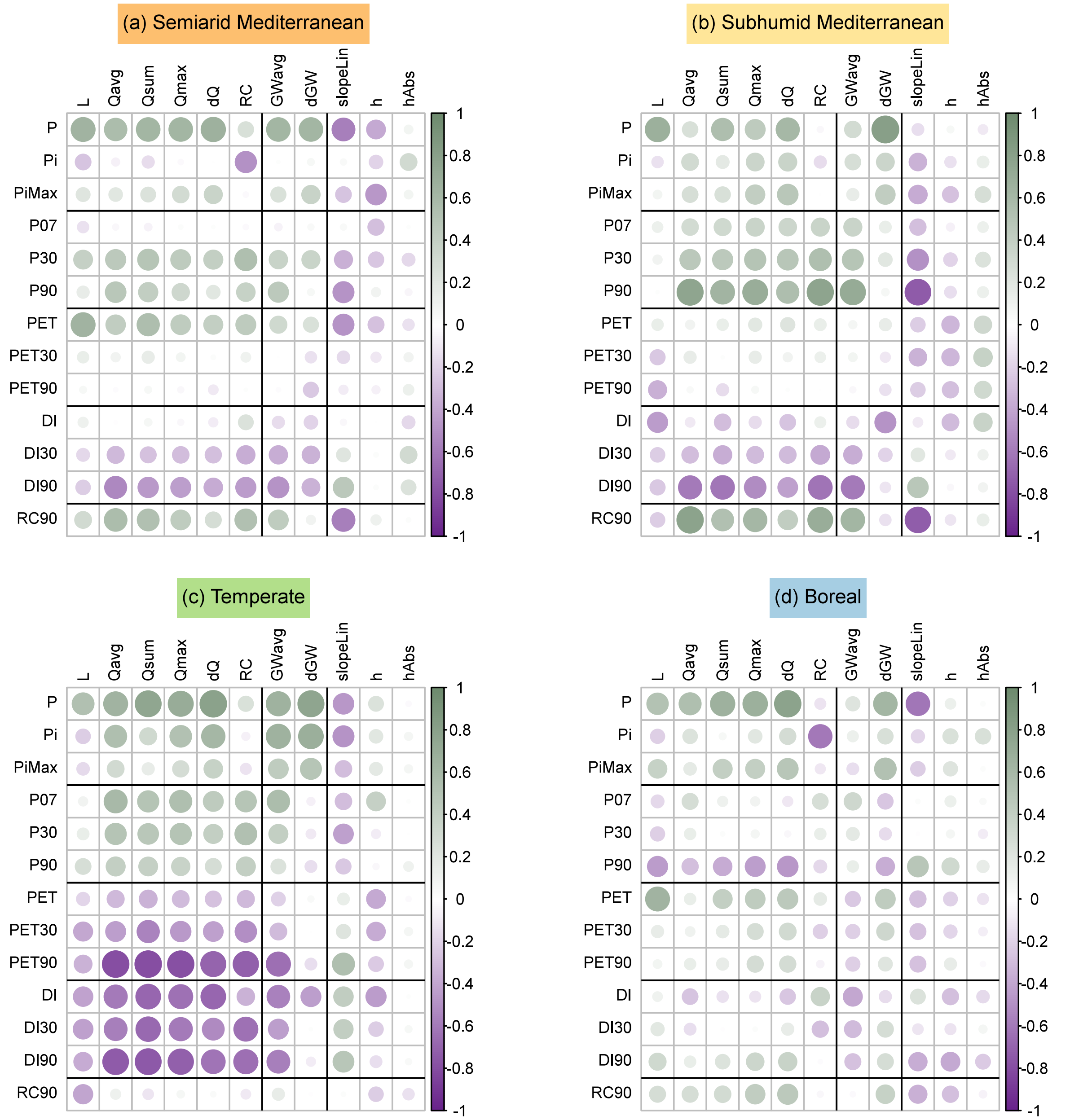

315

Figure 4: Spearman's rank correlation matrices relating hydroclimatic predictors (Table 2) and hydrological response metrics (Table 3) for each catchment. Horizontal and vertical black lines separate predictors and response metrics into specific categories described in Table 2 and Table 3, respectively.

https://doi.org/10.5194/egusphere-2026-4221
Preprint. Discussion started: 17 July 2026
© Author(s) 2026. CC BY 4.0 License.

The mean-weighted explained variance from the MMI models for the stream discharge and groundwater table response metrics ranged from moderate ($0.35 < wR^2 < 0.7$) to, more commonly, high ($wR^2 > 0.7$, Table 4). For these metrics combined, the average wR^2 ± standard deviation was 0.86 ± 0.09 at the semiarid Mediterranean site, 0.56 ± 0.19 at the subhumid Mediterranean site, 0.73 ± 0.14 at the temperate site, and 0.64 ± 0.16 at the boreal site. While wR^2 was similar for discharge and groundwater table metrics at the semiarid site, groundwater responses were relatively better predicted at the subhumid site, and discharge responses were relatively better predicted at the temperate and boreal sites (Table 4). Metrics describing Q-GW relationships generally showed lower explanatory power, especially *hAbs*, which showed wR^2 values ranging from 0.04 to 0.19 across sites.

Table 4: Mean-weighted explained variance (wR^2) of the retained models from the multimodel inference analysis for each hydrological response metric (Table 3) at the four study sites.

Metric	wR^2 Semiarid Mediterranean	wR^2 Subhumid Mediterranean	wR^2 Temperate	wR^2 Boreal
L	0.86	0.79	0.65	0.80
Qavg	0.93	0.44	0.83	0.68
Qsum	0.92	0.37	0.88	0.60
Qmax	0.87	0.41	0.86	0.77
dQ	0.87	0.37	0.82	0.80
RC	0.67	0.54	0.73	0.49
GWavg	0.81	0.76	0.60	0.61
dGW	0.95	0.80	0.49	0.34
slopeLin	0.51	0.43	0.61	0.49
h	0.34	0.16	0.30	0.37
hAbs	0.13	0.19	0.16	0.04

The *slopeLin* response metric showed moderate explained variance across sites, with wR^2 values ranging from 0.43 at the subhumid Mediterranean site to 0.61 at the temperate site (Table 4). At the semiarid Mediterranean site, three predictors (*P*, *P30*, and *RC90*) were retained in the MMI models, all showing negative standardized coefficients, with *P* contributing the most to explained variance (Fig. 5a). At the subhumid Mediterranean site, *slopeLin* was explained by predictors related to rainfall intensity and long-term antecedent conditions (*Pi*, *PiMax*, *P90*, *DI90*, and *RC90*), with *RC90* accounting for the largest share of explained variance and exhibiting a negative relationship with *slopeLin* (Fig. 5b). At the temperate site, six predictors (*Pi*, *P90*, *PET*, *PET90*, *DI*, and *DI30*) were retained, with *PET* explaining the highest proportion of variance and negatively associated with *slopeLin* (Fig. 5c). At the boreal site, *slopeLin* was explained by *P* and, especially, *P90* and *RC90*, which were positively associated with *slopeLin* (Fig. 5d).

https://doi.org/10.5194/egusphere-2026-4221
Preprint. Discussion started: 17 July 2026
© Author(s) 2026. CC BY 4.0 License.

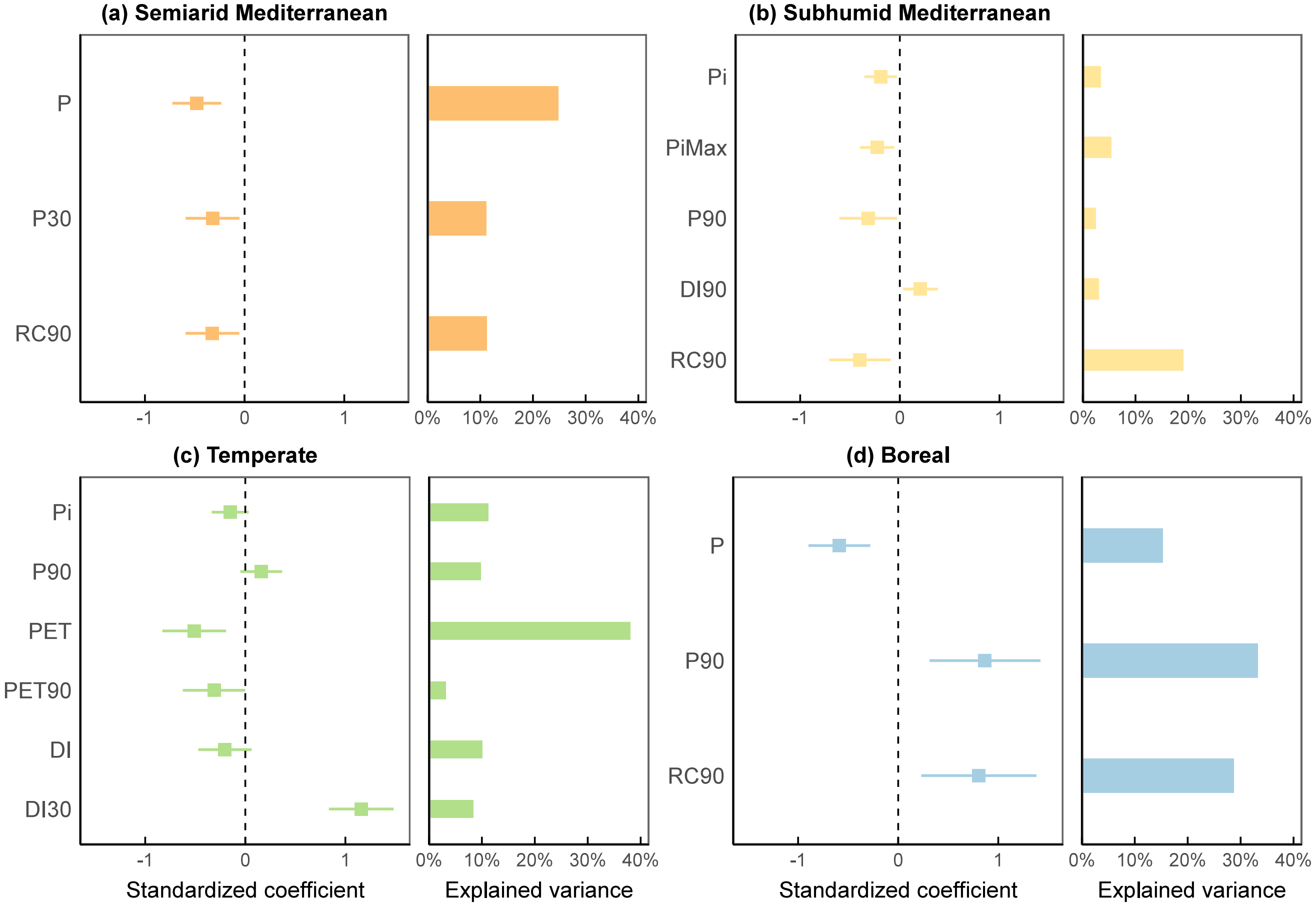

Figure 5: Weighted average of standardized regression coefficients and mean-weighted partitioned variance of predictors (Table 2) from the multimodel inference analysis using *slopeLin* as the response variable. The *slopeLin* represents the linear relationship between stream discharge and riparian groundwater table during rainfall–runoff events. Higher *slopeLin* value reflects a relatively lower effective hydraulic conductivity of the activated riparian layers, as vertical saturation increases its importance relative to the lateral flow. Results are shown for (a) the semiarid Mediterranean, (b) the subhumid Mediterranean, (c) the temperate, and (d) the boreal study sites.

The hysteresis index *h* showed low to moderate explained variance, with wR^2 values ranging from 0.16 at the subhumid Mediterranean site to 0.37 at the boreal site (Table 4). At the semiarid Mediterranean site, four predictors (*Pi*, *PiMax*, *P30*, and *RC90*) were retained, with *Pi* and *P30* contributing the most to explained variance and negatively associated with *h* (Fig. 6a). At the subhumid Mediterranean site, a broad set of predictors was retained, but all showed low (< 10%) individual contributions to explained variance (Fig. 6b). At the temperate site, *P07* was positively associated with *h*, whereas *PET90* and, more strongly, *P30* and *PET* showed negative associations (Fig. 6c). Yet, *P07* also significantly contributed to explained variance and was positively associated with *h*. At the boreal site, *P*, *PiMax*, *P30*, *DI*, and *RC90* were retained, with *RC90* contributing overwhelmingly (30%) to the explained variance and showing a strong negative association with *h* (Fig. 6d).

https://doi.org/10.5194/egusphere-2026-4221
Preprint. Discussion started: 17 July 2026
© Author(s) 2026. CC BY 4.0 License.

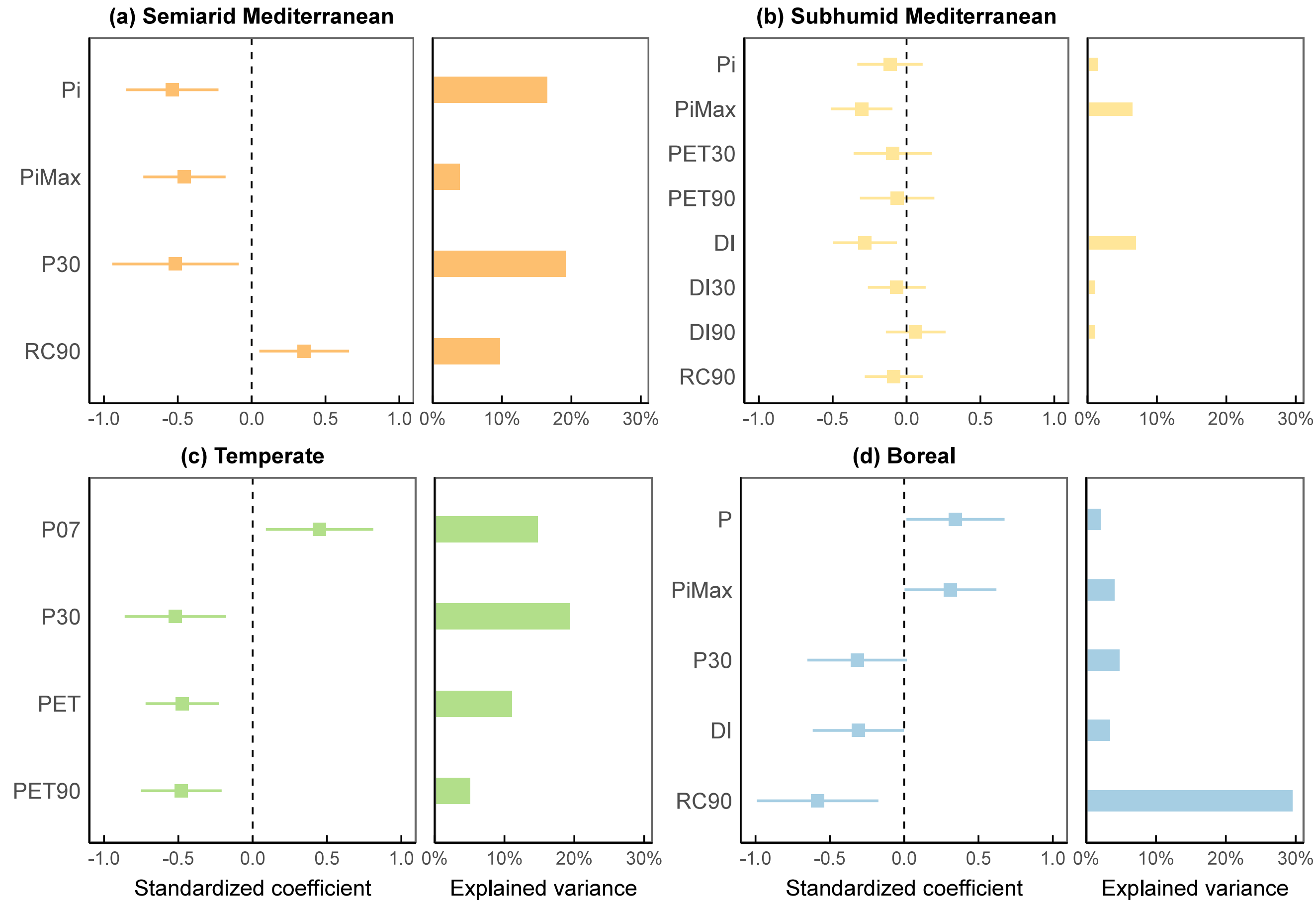

355

Figure 6: Weighted average of standardized regression coefficients and mean-weighted partitioned variance of predictors (Table 2) from the multimodel inference analysis using *h* as the response variable. The metric *h* is the hysteresis index between stream discharge and the riparian groundwater table during rainfall–runoff events. Higher *h* values indicate a relatively faster groundwater response compared to the stream response, regardless of whether *h* is positive or negative. Results are shown for (a) the semiarid Mediterranean, (b) the subhumid Mediterranean, (c) the temperate, and (d) the boreal study sites.

4 Discussion

4.1 Contrasting rainfall–runoff event characteristics and responses across ecoregions

The hydroclimatic contexts of the four study sites strongly shaped the characteristics of rainfall–runoff events and the resulting stream discharge and riparian groundwater table responses. In this subsection, we discuss these general event patterns and the main hydroclimatic factors regulating stream and riparian groundwater dynamics across ecoregions, while Sect. 4.2 focuses specifically on the coupled riparian groundwater–stream dynamics.

Across sites, the observed differences in hydrological behaviour were broadly consistent with their positions along the Budyko framework (Ledesma et al., 2025). Water-limited Mediterranean catchments displayed lower hydrological efficiency

https://doi.org/10.5194/egusphere-2026-4221
Preprint. Discussion started: 17 July 2026
© Author(s) 2026. CC BY 4.0 License.

(i.e., lower *RC* and *RC*90) than the energy-limited temperate and boreal systems. Long-term antecedent conditions (*P90*, *PET90*, *DI90*) were also consistent with this hydroclimatic gradient, reflecting lower water inputs and higher evaporative demand toward the Mediterranean ecoregion. By contrast, *PET* and *DI* showed little variation at the event scale. This likely reflects that rainfall did not generate runoff events during the warmest period at the semiarid Mediterranean site and that snow-affected periods at the temperate and boreal sites were excluded from the analysis, thereby filtering out the most extreme conditions.

Mediterranean sites also experienced rainfall regimes of greater magnitude (*P*) and notably higher intensity (*Pi*), in agreement with regional climatological patterns (Llasat et al., 2010; Marchi et al., 2010). These intense rainfall inputs contribute to the high variability in hydrological responses observed there, particularly at the semiarid site (e.g., *L*, *RC*, *dGW*, *slopeLin*), in line with the erratic flow regimes characteristic of intermittent systems (Botter et al., 2013; Datry et al., 2014). In contrast, temperate and boreal catchments exhibited more persistent responses aligned with their perennial streamflow regimes. Yet, event-based *RC* values were particularly variable at the temperate site with some cases exceeding 100 % (Fig. 3c). Such values could be explained by (i) potential underestimation of rainfall inputs, or (ii) high *P07* during low evapotranspiration periods, whereby short-term antecedent wetness enables substantial water mobilization during subsequent rainfall events. Forest dieback has substantially reduced canopy interception there (Musolff et al., 2024) and could contribute to this behaviour.

Stream discharge and riparian groundwater table responses were primarily driven by rainfall amount across sites, which was consistently selected as an important predictor in the MMI models. These hydrological responses were further modulated by antecedent wetness (*P07*, *P30*, or *P90*), with wetter conditions generally enhancing event responses. These dual controls, event rainfall and antecedent wetness, have been widely documented in event-based studies across ecoregions (e.g., Penna et al., 2011; Ali et al., 2015). Seasonality and aridity were influential at the temperate site, where higher event-based and antecedent *PET* and *DI* dampened hydrological responses. This pattern mirrors observations from other temperate catchments and is consistent with reduced antecedent storage and connectivity during warm, dry periods (Merz and Blöschl, 2009; Tarasova et al., 2018). The greater importance of *PET*- and *DI*-related predictors at the temperate site may reflect the fact that small rainfall events, particularly in summer, often triggered detectable responses, whereas similar events failed to do so in the other catchments (indeed, lower *P* values were associated with the identified events at the temperate site, Fig. 2a). At the boreal site, the more organic, porous soils likely require larger inputs before connectivity is established due to a fill–spill mechanism (Tromp-van Meerveld and McDonnell, 2006). At the Mediterranean sites, larger rainfall amounts are generally needed to generate responses, particularly during drier conditions (Gallart et al., 2002).

Finally, the MMI models showed that groundwater table responses were better predicted than stream discharge responses at the subhumid Mediterranean site, whereas the opposite occurred at the temperate and boreal sites. At the subhumid site, this pattern may arise from a decadal drought, with eight of the years between 2015 and 2024 recording below-average precipitation (Lupon et al., 2018), potentially altering upslope contributions and reducing the explanatory power for stream discharge responses. At the temperate and boreal sites, some events occurred when the riparian groundwater table was

https://doi.org/10.5194/egusphere-2026-4221
Preprint. Discussion started: 17 July 2026
© Author(s) 2026. CC BY 4.0 License.

already close to the soil surface, limiting the capacity for further rise and potentially weakening linear relationships with hydroclimatic predictors relative to stream discharge. These contrasting patterns underscore the inherently different hydrological processes across the studied ecoregions.

4.2 Drivers of riparian–stream hydrological interactions across ecoregions

Hydrological response metrics that integrate stream discharge and riparian groundwater dynamics provided additional insights into runoff generation mechanisms across the four ecoregions represented by our study sites. In this subsection, we focus on the *slopeLin* and *h* metrics to examine how riparian–stream interactions differ among sites and how these interactions are shaped by hydroclimatic drivers.

We used the *slopeLin* metric as a proxy for the effective average hydraulic conductivity of the riparian layers activated during rainfall–runoff events. At the Mediterranean sites, deeper, more mineral and therefore less conductive riparian layers are typically activated during events (Butturini et al., 2003). Accordingly, the median rise in riparian groundwater (*dGW*) is generally low (Fig. 3d), likely because a substantial fraction of rainfall does not infiltrate to those depths. When recharge does occur, however, vertical saturation can develop rapidly, as low lateral connectivity amplifies vertical filling, particularly at the more erratic semiarid Mediterranean site. These structural differences help explain why rainfall amount, antecedent wetness, and hydrological efficiency emerged as dominant predictors of *slopeLin* at the Mediterranean sites. Only under sufficiently wet antecedent conditions followed by adequate rainfall are the more conductive upper riparian layers hydrologically activated.

In contrast, lower *slopeLin* values at the temperate and boreal sites indicate higher effective conductivity (Fig. 3e), consistent with riparian groundwater tables that are generally closer to the surface and drain organic, porous soil layers (Ledesma et al., 2015; Werner et al., 2021). At the boreal site, event rainfall was associated with lower *slopeLin* values, consistent with the activation of highly conductive near-surface layers. However, *slopeLin* increased with wetter antecedent states (*P90*, *RC90*), suggesting that under already wet and hydrologically efficient conditions, additional rainfall either (i) raised the groundwater table further without substantially enhancing lateral transmissivity, producing a stronger filling signal relative to lateral flow, or (ii) activated hydrological connectivity with water sources beyond the riparian zone (Zimmer and McGlynn, 2018; Bishop et al., 2024).

At the temperate site, *slopeLin* decreased with increasing *PET*, implying that more conductive layers were active during warmer periods. Within the *slopeLin* framework alone, this pattern appears counterintuitive, as warmer conditions are typically associated with deeper groundwater tables residing in more mineral, less conductive layers. Integrating this result with the *h* index clarifies the underlying mechanism. Events occurring during warm periods, particularly when preceded by a wet month, were associated with lower *h* values, indicating relatively faster stream responses. This suggests that under these conditions the riparian zone contributes little to the event response, while the stream still reacts rapidly to rainfall inputs, likely driven by other water sources such as upstream tributaries or a spring that continuously feeds the system. Such

https://doi.org/10.5194/egusphere-2026-4221
Preprint. Discussion started: 17 July 2026
© Author(s) 2026. CC BY 4.0 License.

behaviour is consistent with seasonal shifts in dominant flow pathways and spatially variable source-area activation in temperate catchments (Tetzlaff et al., 2013).

Outside these seasonal conditions, the dominant hysteresis pattern at both the temperate and boreal sites was clockwise, indicating that the riparian zone generally responds first to rainfall inputs and the stream follows. This pattern represents a classical response sequence in temperate and northern headwaters where near-stream, conductive soil layers strongly control runoff generation (McGlynn and McDonnell, 2003; Bishop et al., 2004; Frei et al., 2010). At the boreal site, high hydrological efficiency (*RC90*) was associated with relatively faster stream responses, likely reflecting the influence of the preceding snowmelt period, which enhances hydrological connectivity with upslope parts of the catchment beyond the riparian zone (Laudon et al., 2004).

In contrast, the Mediterranean sites did not exhibit the classical clockwise riparian–stream response sequence. Instead, hysteresis patterns were weak or absent at the semiarid site and predominantly anticlockwise at the subhumid site. The generally synchronous response at the semiarid site likely reflects a combination of vertical filling of low-conductive riparian layers, which only partially feed the stream, and additional contributions from upstream sources or perched groundwater tables (Butturini et al., 2003). At the subhumid site, the generally faster stream response relative to the riparian response is more striking, as it resembles neither the temperate site nor its Mediterranean counterpart. This apparent lack of early riparian–stream connectivity is consistent with the reduced explained variance of stream discharge responses. It likely involves an increased contribution of fast upslope or subsurface flow pathways during event onset, as documented for similar Montseny catchments (Àvila et al., 1992), with recent drought conditions potentially enhancing this behaviour.

At both Mediterranean sites, events characterized by high rainfall intensity following wet antecedent conditions were associated with relatively faster stream responses. Under such circumstances, we hypothesize that the rapid activation of small ephemeral tributaries becomes the dominant runoff generation mechanism, at least during the initial phase of events. Ephemeral stream networks are known to respond rapidly to intense rainfall, particularly when antecedent wetness facilitates the reconnection of otherwise disconnected flow pathways and channel segments (Azarnivand et al., 2020).

Finally, it is worth noting that the MMI models showed only low to moderate explanatory power for the *h* index, while performance for hAbs, which quantifies the magnitude of timing discrepancies between stream and riparian groundwater responses, was generally poor. This likely reflects the strong nonlinearity inherent to processes governing response timing, which may not be well captured by linear model structures. Moreover, while rainfall amount consistently explained individual stream and riparian groundwater responses, it rarely emerged as a key driver of their integrated behaviour, highlighting that additional, site-specific drivers (e.g., rainfall intensity, seasonality, antecedent hydrological efficiency) become dominant when analysing complex hydrological interactions (Hövel et al., 2025).

4.3 Implications for solute mobilization and concluding remarks

Ecoregion-specific stream and riparian groundwater responses to rainfall events, and their associated connectivity and hysteresis patterns, underpin implications for solute mobilization. The *slopeLin* and *h* index metrics presented here, based on

https://doi.org/10.5194/egusphere-2026-4221
Preprint. Discussion started: 17 July 2026
© Author(s) 2026. CC BY 4.0 License.

two easily measurable hydrological variables, offer a simple yet informative framework to interpret runoff generation mechanisms, which are fundamental for understanding solute mobilization in headwater catchments. While uncertainties remain, particularly potential timing offsets between rainfall and observation records, as well as differences in catchment size and spatial heterogeneity within catchments, our approach captured first-order drivers of coupled stream and riparian groundwater responses across ecoregions that are otherwise difficult to quantify. Unlike commonly applied hysteresis analyses of concentration–discharge (*c*–*Q*) relationships (Knapp and Musolff, 2024; Speir et al., 2024), which describe the mobilization of solutes already present in the system, the *h* index used here focuses on the physical connectivity between the riparian zone and the stream that enables such mobilization. Still, both perspectives are complementary, and together they can provide an integrated understanding of how hydrological activation and solute sources interact during rainfall–runoff events.

These processes can be interpreted along two complementary aspects of hydrological connectivity. When the riparian zone is connected to the stream and acts as the main driver of the hydrological response, the vertical sequence and depth of layer activation strongly control which solutes are mobilized and when during an event (Stewart et al., 2022; Ledesma et al., 2025), thereby shaping stream chemistry and associated *c*–*Q* relationships. Conversely, when the riparian zone is disconnected or not the dominant driver of stream response, other water sources govern solute mobilization and redefine *c*–*Q* relationships. As previously suggested, the riparian zone does not consistently control stream chemistry across all hydrological conditions (Ledesma et al., 2025), and the results presented here provide a hydrological explanation for why this is the case during rainfall–runoff events.

At the semiarid Mediterranean site, rainfall–runoff events typically activate deep, mineral, and low-conductive riparian layers, which only reach shallower and more organic conductive layers when rainfall and antecedent wetness are sufficient. Although positive relationships between stream discharge and solutes such as dissolved organic carbon (DOC) or nitrate (NO_3^-) are consistent with this vertical activation (Bernal et al., 2002; Ledesma et al., 2025), these relationships are usually weak and not systematic. As shown here, this likely reflects that while riparian and stream responses are often synchronous, high-intensity events can disrupt this coupling by activating other water sources before or in addition to the riparian zone (Butturini et al., 2008). At the subhumid Mediterranean site, the situation is even more complex. Despite previous studies reporting positive DOC and NO_3^- *c*–*Q* relationships and highlighting a riparian influence (Bernal et al., 2019; Ledesma et al., 2022), our results indicate that solute mobilization during events cannot be consistently attributed to the riparian zone alone. Instead, the hydrological disconnection identified here suggests that additional sources, such as ephemeral tributaries, may intermittently contribute to streamflow, complicating the interpretation of *c*–*Q* relationships. An increasing prevalence of intense rainfall events may further disrupt *c*–*Q* relationships at Mediterranean sites by favouring the activation of non-riparian sources, thereby increasing the likelihood of riparian–stream disconnection.

At the temperate and boreal sites, the narrow and shallow riparian layers activated during rainfall–runoff events become progressively more organic toward the surface. Their activation, together with the prevalent clockwise riparian–stream response patterns, is consistent with the classical sequence of solute mobilization, whereby rising DOC concentrations are

https://doi.org/10.5194/egusphere-2026-4221
Preprint. Discussion started: 17 July 2026
© Author(s) 2026. CC BY 4.0 License.

driven by riparian inputs (Ledesma et al., 2015; Musolff et al., 2018). This interpretation, however, breaks down under specific conditions. At the temperate site, seasonality exerts a strong control on hydrological responses, such that during warm periods the riparian zone appears temporarily disconnected from the stream, allowing upstream tributaries to dominate runoff generation. This behaviour is consistent with observations from other temperate catchments, where DOC mobilization is inhibited under warm, dry conditions (Blaurock et al., 2021). At the boreal site, snowmelt exerts long-lasting effects that enhance connectivity with upslope sources and can induce solute source limitation within the riparian zone, thereby diluting the riparian chemical signal (Laudon et al., 2004). Under warmer and drier conditions, seasonal disconnection at the temperate site and reduced snowmelt influence at the boreal site could modify riparian–stream interactions, with implications for solute mobilization and stream chemistry.

This study revealed that riparian–stream linkages, often assumed to dominate headwater hydrology and biogeochemistry, are contingent and variable across ecoregions and rainfall–runoff events. Recognizing when and how this connectivity emerges provides a clearer framework for understanding solute mobilization and for refining conceptual models of catchment functioning across ecoregions.

https://doi.org/10.5194/egusphere-2026-4221
Preprint. Discussion started: 17 July 2026
© Author(s) 2026. CC BY 4.0 License.

Appendix A: spatial consistency of riparian groundwater observations

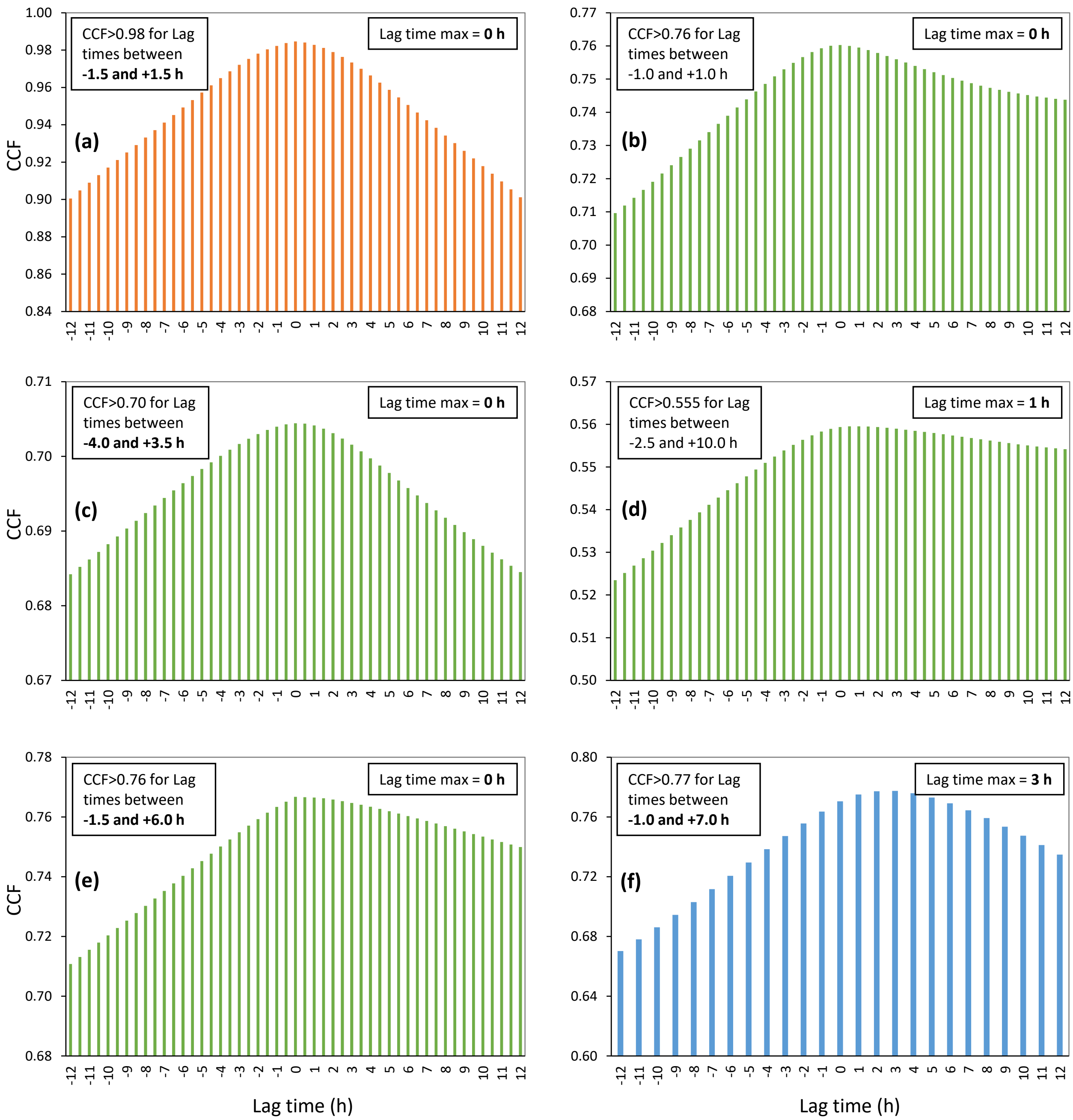

Figure A1. Cross-correlation function (CCF) between riparian groundwater table in the monitoring wells used in this study and those in adjacent monitoring wells representing the riparian zone at each study site. CCFs are plotted at 30-minute lag intervals for (a) the semiarid Mediterranean *Fuirosos* and (b), (c), (d), (e) the temperate *Upper Rappbode*, and at 1-hour intervals for (f) the boreal *Krycklan C2*. Note that no adjacent monitoring well data were available for the subhumid Mediterranean *Font del Regàs* at the same resolution as the studied well, but groundwater table dynamics at this well were shown to be similar to those measured at seven other adjacent wells with ca. biweekly data from September 2010 to August 2012 (Ledesma et al., 2021b).

https://doi.org/10.5194/egusphere-2026-4221
Preprint. Discussion started: 17 July 2026
© Author(s) 2026. CC BY 4.0 License.

Appendix B: frequency of hysteresis pattern types

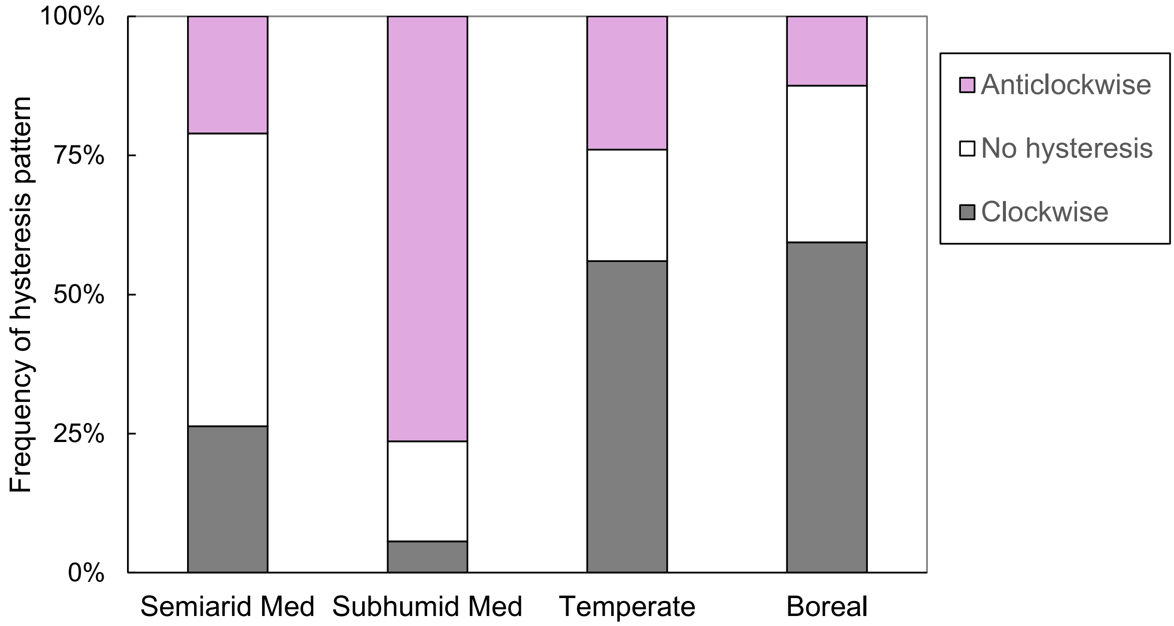

Figure B1. Frequency of hysteresis pattern types relative to the total number of rainfall–runoff events identified at each study site.

Data availability

The event-level dataset underlying the statistical analyses and figures is available in HydroShare (Ledesma, 2026), https://doi.org/10.4211/hs.17075f4b1f874f389c69f1f491bdafdb.

Author contributions

José L. J. Ledesma: Conceptualization, Data curation, Formal analysis, Funding acquisition, Investigation, Methodology, Project administration, Visualization, Writing – original draft, Writing – review & editing. **Paul D. Burkhardt:** Data curation, Investigation, Writing – review & editing. **Susana Bernal:** Conceptualization, Data curation, Investigation, Writing – review & editing. **Andreas Musolff:** Conceptualization, Data curation, Investigation, Writing – review & editing.

Competing interests

The authors declare that they have no conflict of interest.

© Author(s) 2026. CC BY 4.0 License.

Disclaimer

Copernicus Publications remains neutral with regard to jurisdictional claims made in the text, published maps, institutional affiliations, or any other geographical representation in this paper. While Copernicus Publications makes every effort to include appropriate place names, the final responsibility lies with the authors. Views expressed in the text are those of the authors and do not necessarily reflect the views of the publisher.

Acknowledgements

During manuscript preparation, the authors used ChatGPT (OpenAI) to assist with the technical refinement and troubleshooting of R code used to generate figures. The tool was also used for sentence-level language editing limited to improving clarity, grammar, and readability. All code and text were critically reviewed and validated by the authors. The tool was not used to generate data, results, or scientific interpretations, and the authors take full responsibility for the manuscript. We thank Montserrat Soler, Xavier Peñarroya, Carolina Jativa, and Anna Lupon for data collection and pre-processing at the *Fuirosos* and *Font del Regàs* sites, and Toralf Keller for data collection and pre-processing at the *Rappbode* catchment. We also acknowledge the Reference Climate Monitoring Program at SLU Experimental Forests and SITES Svartberget for providing high-frequency precipitation data from *Krycklan*, and Rebeca Arias-Real for guidance on the multimodel inference methodology.

Financial support

JLJL was supported by a Ramón y Cajal grant (RYC2022-035220-I) funded by MICIU/AEI/10.13039/501100011033 and FSE+. PDB's work was supported by the project SUDOCQU (LE 5028/2-1) funded by the *Deutsche Forschungsgemeinschaft* (DFG) / 10.13039/501100001659. SB's work was supported by the projects EVASIONA (PID2021-122817-NB-I00), RIPAMED (CNS2023-144737), and OXIT (PID2024-158111NB-C21) funded by MICIU/AEI/10.13039/501100011033, FEDER, UE and Next Generation EU/PRTR.

References

Ali, G., Tetzlaff, D., McDonnell, J. J., Soulsby, C., Carey, S., Laudon, H., McGuire, K., Buttle, J., Seibert, J., and Shanley, J.: Comparison of threshold hydrologic response across northern catchments, Hydrological Processes, 29, 3575-3591, https://doi.org/10.1002/hyp.10527, 2015.

Allen, R. G., Pereira, L. S., Raes, D., and Smith, M.: Crop evapotranspiration - Guidelines for computing crop water requirements - FAO Irrigation and drainage paper 56, Rome, 1998.

https://doi.org/10.5194/egusphere-2026-4221
Preprint. Discussion started: 17 July 2026
© Author(s) 2026. CC BY 4.0 License.

Àvila, A., Piñol, J., Rodà, F., and Neal, C.: Storm solute behavior in a montane Mediterranean forested catchment, Journal of Hydrology, 140, 143–161, https://doi.org/10.1016/0022-1694(92)90238-q, 1992.

Azarnivand, A., Camporese, M., Alaghmand, S., and Daly, E.: Simulated response of an intermittent stream to rainfall frequency patterns, Hydrological Processes, 34, 615–632, https://doi.org/10.1002/hyp.13610, 2020.

Bartoń, K.: MuMIn: Multi-Model Inference, R package version 1.48.11, https://CRAN.R-project.org/package=MuMIn, 2025.

Beiter, D., Weiler, M., and Blume, T.: Characterising hillslope-stream connectivity with a joint event analysis of stream and groundwater levels, Hydrology and Earth System Sciences, 24, 5713–5744, https://doi.org/10.5194/hess-24-5713-2020, 2020.

Bernal, S., Butturini, A., and Sabater, F.: Variability of DOC and nitrate responses to storms in a small Mediterranean forested catchment, Hydrology and Earth System Sciences, 6, 1031–1041, https://doi.org/10.5194/hess-6-1031-2002, 2002.

Bernal, S., Lupon, A., Wollheim, W. M., Sabater, F., Poblador, S., and Martí, E.: Supply, Demand, and In-Stream Retention of Dissolved Organic Carbon and Nitrate During Storms in Mediterranean Forested Headwater Streams, Frontiers in Environmental Science, 7, 60, https://doi.org/10.3389/fenvs.2019.00060, 2019.

Beven, K.: Towards a methodology for testing models as hypotheses in the inexact sciences, Proceedings of the Royal Society a-Mathematical Physical and Engineering Sciences, 475, 20180862, https://doi.org/10.1098/rspa.2018.0862, 2019.

Bishop, K., Seibert, J., Köhler, S., and Laudon, H.: Resolving the Double Paradox of rapidly mobilized old water with highly variable responses in runoff chemistry, Hydrological Processes, 18, 185–189, https://doi.org/10.1002/hyp.5209, 2004.

Bishop, K., Ameli, A., Grabs, T., Laudon, H., Amvrosiadi, N., Kolbe, T., Seibert, J., and van Meerveld, I.: Identifying Subsurface Connectivity From Observations: Experimentation With Equifinality Defines Both Challenges and Pathways to Progress, Hydrological Processes, 38, e15324, https://doi.org/10.1002/hyp.15324, 2024.

Blaurock, K., Beudert, B., Gilfedder, B. S., Fleckenstein, J. H., Peiffer, S., and Hopp, L.: Low hydrological connectivity after summer drought inhibits DOC export in a forested headwater catchment, Hydrology and Earth System Sciences, 25, 5133–5151, https://doi.org/10.5194/hess-25-5133-2021, 2021.

Blöschl, G., Bierkens, M. F. P., Chambel, A., Cudennec, C., Destouni, G., Fiori, A., Kirchner, J. W., McDonnell, J. J., Savenije, H. H. G., Sivapalan, M., Stumpp, C., Toth, E., Volpi, E., Carr, G., Lupton, C., Salinas, J., Szeles, B., Viglione, A., Aksoy, H., Allen, S. T., Amin, A., Andreassian, V., Arheimer, B., Aryal, S. K., Baker, V., Bardsley, E., Barendrecht, M. H., Bartosova, A., Batelaan, O., Berghuijs, W. R., Beven, K., Blume, T., Bogaard, T., de Amorim, P. B., Bottcher, M. E., Boulet, G., Breinl, K., Brilly, M., Brocca, L., Buytaert, W., Castellarin, A., Castelletti, A., Chen, X. H., Chen, Y. B., Chen, Y. F., Chifflard, P., Claps, P., Clark, M. P., Collins, A. L., Croke, B., Dathe, A., David, P. C., de Barros, F. P. J., de Rooij, G., Di Baldassarre, G., Driscoll, J. M., Duethmann, D., Dwivedi, R., Eris, E., Farmer, W. H., Feiccabrino, J., Ferguson, G., Ferrari, E., Ferraris, S., Fersch, B., Finger, D., Foglia, L., Fowler, K., Gartsman, B., Gascoin, S., Gaume, E., Gelfan, A., Geris, J., Gharari, S., Gleeson, T., Glendell, M., Bevacqua, A. G., Gonzalez-Dugo, M. P., Grimaldi, S., Gupta, A. B., Guse, B., Han, D. W., Hannah, D., Harpold, A., Haun, S., Heal, K., Helfricht, K., Herrnegger, M., Hipsey, M., Hlavacikova, H.,

https://doi.org/10.5194/egusphere-2026-4221
Preprint. Discussion started: 17 July 2026
© Author(s) 2026. CC BY 4.0 License.

Hohmann, C., Holko, L., Hopkinson, C., Hrachowitz, M., Illangasekare, T. H., Inam, A., Innocente, C., Istanbulluoglu, E., Jarihani, B., Kalantari, Z., Kalvans, A., Khanal, S., Khatami, S., Kiesel, J., Kirkby, M., Knoben, W., Kochanek, K., Kohnova, S., Kolechkina, A., Krause, S., Kreamer, D., Kreibich, H., Kunstmann, H., Lange, H., Liberato, M. L. R., Lindquist, E., Link, T., Liu, J. G., Loucks, D. P., Luce, C., Mahe, G., Makarieva, O., Malard, J., Mashtayeva, S., Maskey, S., Mas-Pla, J., Mavrova-Guirguinova, M., Mazzoleni, M., Mernild, S., Misstear, B. D., Montanari, A., Muller-Thomy, H., Nabizadeh, A., Nardi, F., Neale, C., Nesterova, N., Nurtaev, B., Odongo, V. O., Panda, S., Pande, S., Pang, Z. H., Papacharalampous, G., Perrin, C., Pfister, L., Pimentel, R., Polo, M. J., Post, D., Sierra, C. P., Ramos, M. H., Renner, M., Reynolds, J. E., Ridolfi, E., Rigon, R., Riva, M., Robertson, D. E., Rosso, R., Roy, T., Sa, J. H. M., Salvadori, G., Sandells, M., Schaefli, B., Schumann, A., Scolobig, A., Seibert, J., Servat, E., Shafiei, M., Sharma, A., Sidibe, M., Sidle, R. C., Skaugen, T., Smith, H., Spiessl, S. M., Stein, L., Steinsland, I., Strasser, U., Su, B., Szolgay, J., Tarboton, D., Tauro, F., Thirel, G., Tian, F. Q., Tong, R., Tussupova, K., Tyralis, H., Uijlenhoet, R., van Beek, R., van der Ent, R. J., van der Ploeg, M., Van Loon, A. F., van Meerveld, I., van Nooijen, R., van Oel, P. R., Vidal, J. P., von Freyberg, J., Vorogushyn, S., Wachniew, P., Wade, A. J., Ward, P., Westerberg, I. K., White, C., Wood, E. F., Woods, R., Xu, Z. X., Yilmaz, K. K., and Zhang, Y. Q.: Twenty-three unsolved problems in hydrology (UPH) - a community perspective, Hydrological Sciences Journal-Journal Des Sciences Hydrologiques, 64, 1141-1158, https://doi.org/10.1080/02626667.2019.1620507, 2019.

Botter, G., Basso, S., Rodriguez-Iturbe, I., and Rinaldo, A.: Resilience of river flow regimes, Proceedings of the National Academy of Sciences of the United States of America, 110, 12925–12930, https://doi.org/10.1073/pnas.1311920110, 2013.

Burnham, K. P. and Anderson, D. R.: Model Selection and Multimodel Inference: A Practical Information-Theoretic Approach, 2nd edn., Springer, https://doi.org/10.1007/b97636, 2002.

Buttle, J.: Mapping first-order controls on streamflow from drainage basins: the T3 template, Hydrological Processes, 20, 3415–3422, https://doi.org/10.1002/hyp.6519, 2006.

Butturini, A., Bernal, S., Nin, E., Hellin, C., Rivero, L., Sabater, S., and Sabater, F.: Influences of the stream groundwater hydrology on nitrate concentration in unsaturated riparian area bounded by an intermittent Mediterranean stream, Water Resources Research, 39, 1110, https://doi.org/10.1029/2001wr001260, 2003.

Butturini, A., Alvarez, M., Bernal, S., Vazquez, E., and Sabater, F.: Diversity and temporal sequences of forms of DOC and NO3-discharge responses in an intermittent stream: Predictable or random succession? Journal of Geophysical Research-Biogeosciences, 113, G03016, https://doi.org/10.1029/2008jg000721, 2008.

Carey, S. K., Tetzlaff, D., Seibert, J., Soulsby, C., Buttle, J., Laudon, H., McDonnell, J., McGuire, K., Caissie, D., Shanley, J., Kennedy, M., Devito, K., and Pomeroy, J. W.: Inter-comparison of hydro-climatic regimes across northern catchments: synchronicity, resistance and resilience, Hydrological Processes, 24, 3591-3602, https://doi.org/10.1002/hyp.7880, 2010.

Datry, T., Larned, S. T., and Tockner, K.: Intermittent Rivers: A Challenge for Freshwater Ecology, Bioscience, 64, 229-235, https://doi.org/10.1093/biosci/bit027, 2014.

Fovet, O., Ruiz, L., Hrachowitz, M., Faucheux, M., and Gascuel-Odoux, C.: Hydrological hysteresis and its value for assessing process consistency in catchment conceptual models, Hydrology and Earth System Sciences, 19, 105–123, https://doi.org/10.5194/hess-19-105-2015, 2015.

Frei, S., Lischeid, G., and Fleckenstein, J. H.: Effects of micro-topography on surface-subsurface exchange and runoff generation in a virtual riparian wetland – A modeling study, Advances in Water Resources, 33, 1388–1401, https://doi.org/10.1016/j.advwatres.2010.07.006, 2010.

Gallart, F., Llorens, P., Latron, J., and Regüés, D.: Hydrological processes and their seasonal controls in a small Mediterranean mountain catchment in the Pyrenees, Hydrology and Earth System Sciences, 6, 527–537, https://doi.org/10.5194/hess-6-527-2002, 2002.

Gelmini, Y., Zuecco, G., Zaramella, M., Penna, D., and Borga, M.: Hysteresis in streamflow-water table relation provides a new classification system of rainfall-runoff events, Hydrological Processes, 36, e14685, https://doi.org/10.1002/hyp.14685, 2022.

Giani, G., Tarasova, L., Woods, R. A., and Rico-Ramirez, M. A.: An Objective Time-Series-Analysis Method for Rainfall-Runoff Event Identification, Water Resources Research, 58, e2021WR031283, https://doi.org/10.1029/2021wr031283, 2022.

Gomi, T., Sidle, R. C., Miyata, S., Kosugi, K., and Onda, Y.: Dynamic runoff connectivity of overland flow on steep forested hillslopes: Scale effects and runoff transfer, Water Resources Research, 44, W08411, https://doi.org/10.1029/2007wr005894, 2008.

Hoffman, G. E., and Schadt, E. E.: variancePartition: interpreting drivers of variation in complex gene expression studies, BMC Bioinformatics, 17, 483, https://doi.org/10.1186/s12859-016-1323-z, 2016.

Hövel, A., Stumpp, C., Bogena, H., Lücke, A., Strauss, P., Blöschl, G., and Stockinger, M.: Hydro-Meteorological Drivers of Event Runoff Characteristics Under Analogous Soil Moisture Patterns in Three Small-Scale Headwater Catchments, Hydrological Processes, 39, e70173, https://doi.org/10.1002/hyp.70173, 2025.

Hughes, D. A., and Metzler, W.: Assessment of three monthly rainfall-runoff models for estimating the water resource yield of semiarid catchments in Namibia, Hydrological Sciences Journal-Journal Des Sciences Hydrologiques, 43, 283–297, https://doi.org/10.1080/02626669809492122, 1998.

Jung, M., Burt, T. P., and Bates, P. D.: Toward a conceptual model of floodplain water table response, Water Resources Research, 40, W12409, https://doi.org/10.1029/2003wr002619, 2004.

Kong, X. Z., Ghaffar, S., Determann, M., Friese, K., Jomaa, S., Mi, C. X., Shatwell, T., Rinke, K., and Rode, M.: Reservoir water quality deterioration due to deforestation emphasizes the indirect effects of global change, Water Research, 221, 118721, https://doi.org/10.1016/j.watres.2022.118721, 2022.

Knapp, J. L. A., and Musolff, A.: Concentration-Discharge Relationships Revisited: Overused But Underutilised? Hydrological Processes, 38(11), e15328, https://doi.org/10.1002/hyp.15328, 2024.

Knapp, J. L. A., Berghuijs, W. R., Floriancic, M. G., and Kirchner, J. W.: Catchment hydrological response and transport are affected differently by precipitation intensity and antecedent wetness, Hydrology and Earth System Sciences, 29, 3673–3685, https://doi.org/10.5194/hess-29-3673-2025, 2025.

Laudon, H., Seibert, J., Köhler, S., and Bishop, K.: Hydrological flow paths during snowmelt: Congruence between hydrometric measurements and oxygen 18 in meltwater, soil water, and runoff, Water Resources Research, 40(3), W03102, https://doi.org/10.1029/2003wr002455, 2004.

Laudon, H., Sponseller, R. A., and Bishop, K.: From legacy effects of acid deposition in boreal streams to future environmental threats, Environmental Research Letters, 16, 015007, https://doi.org/10.1088/1748-9326/abd064, 2021.

Ledesma, J. L. J.: Event-level hydroclimatic and hydrological data for 209 rainfall–runoff events across four forest headwater catchments, HydroShare [data set], https://doi.org/10.4211/hs.17075f4b1f874f389c69f1f491bdafdb, 2026.

Ledesma, J. L. J., Grabs, T., Bishop, K. H., Schiff, S. L., and Köhler, S. J.: Potential for long-term transfer of dissolved organic carbon from riparian zones to streams in boreal catchments, Global Change Biology, 21, 2963–2979, https://doi.org/10.1111/gcb.12872, 2015.

Ledesma, J. L. J., Lupon, A., and Bernal, S.: Hydrological responses to rainfall events including the extratropical cyclone Gloria in two contrasting Mediterranean headwaters in Spain; the perennial Font del Regàs and the intermittent Fuirosos, Hydrological Processes, 35, e14451, https://doi.org/10.1002/hyp.14451, 2021a.

Ledesma, J. L. J., Ruiz-Pérez, G., Lupon, A., Poblador, S., Futter, M. N., Sabater, F., and Bernal, S.: Future changes in the Dominant Source Layer of riparian lateral water fluxes in a subhumid Mediterranean catchment, Journal of Hydrology, 595, 126014, https://doi.org/10.1016/j.jhydrol.2021.126014, 2021b.

Ledesma, J. L. J., Lupon, A., Martí, E., and Bernal, S.: Hydrology and riparian forests drive carbon and nitrogen supply and DOC:NO3- stoichiometry along a headwater Mediterranean stream, Hydrology and Earth System Sciences, 26, 4209–4232, https://doi.org/10.5194/hess-26-4209-2022, 2022.

Ledesma, J. L. J., Musolff, A., Sponseller, R. A., Lupon, A., Peñarroya, X., Jativa, C., and Bernal, S.: The Riparian Zone Controls Headwater Hydrology and Biogeochemistry, Doesn't It? Reassessing Linkages Across European Ecoregions, Global Biogeochemical Cycles, 39, e2024GB008250, https://doi.org/10.1029/2024gb008250, 2025.

Llasat, M. C., Llasat-Botija, M., Prat, M. A., Porcú, F., Price, C., Mugnai, A., Lagouvardos, K., Kotroni, V., Katsanos, D., Michaelides, S., Yair, Y., Savvidou, K., and Nicolaides, K.: High-impact floods and flash floods in Mediterranean countries: the FLASH preliminary database, Advances in Geosciences, 23, 47-55, https://doi.org/10.5194/adgeo-23-47-2010, 2010.

Lupon, A., Sabater, F., Miñarro, A., and Bernal, S.: Contribution of pulses of soil nitrogen mineralization and nitrification to soil nitrogen availability in three Mediterranean forests, European Journal of Soil Science, 67, 303–313, https://doi.org/10.1111/ejss.12344, 2016.

Lupon, A., Ledesma, J. L. J., and Bernal, S.: Riparian evapotranspiration is essential to simulate streamflow dynamics and water budgets in a Mediterranean catchment, Hydrology and Earth System Sciences, 22, 4033–4045, https://doi.org/10.5194/hess-22-4033-2018, 2018.

© Author(s) 2026. CC BY 4.0 License.

Marchi, L., Borga, M., Preciso, E., and Gaume, E.: Characterisation of selected extreme flash floods in Europe and implications for flood risk management, Journal of Hydrology, 394, 118–133, https://doi.org/10.1016/j.jhydrol.2010.07.017, 2010.

Martínez-Carreras, N., Wetzel, C. E., Frentress, J., Ector, L., McDonnell, J. J., Hoffmann, L., and Pfister, L.: Hydrological connectivity inferred from diatom transport through the riparian-stream system, Hydrology and Earth System Sciences, 19, 3133–3151, https://doi.org/10.5194/hess-19-3133-2015, 2015.

McGlynn, B. L., and McDonnell, J. J.: Quantifying the relative contributions of riparian and hillslope zones to catchment runoff, Water Resources Research, 39(11), 1310, https://doi.org/10.1029/2003wr002091, 2003.

Merz, R., and Blöschl, G.: A regional analysis of event runoff coefficients with respect to climate and catchment characteristics in Austria, Water Resources Research, 45, W01405, https://doi.org/10.1029/2008wr007163, 2009.

Montgomery, D. C., Peck, E. A., and Vining, G. G.: Introduction to Linear Regression Analysis, 5th edn., John Wiley & Sons, Hoboken, New Jersey, USA, 2012.

Musolff, A., Fleckenstein, J. H., Opitz, M., Büttner, O., Kumar, R., and Tittel, J.: Spatio-temporal controls of dissolved organic carbon stream water concentrations, Journal of Hydrology, 566, 205–215, https://doi.org/10.1016/j.jhydrol.2018.09.011, 2018.

Musolff, A., Zhan, Q., Dupas, R., Minaudo, C., Fleckenstein, J. H., Rode, M., Dehaspe, J., and Rinke, K.: Spatial and Temporal Variability in Concentration-Discharge Relationships at the Event Scale, Water Resources Research, 57, e2020WR029442, https://doi.org/10.1029/2020wr029442, 2021.

Musolff, A., Tarasova, L., Rinke, K., and Ledesma, J. L. J.: Forest Dieback Alters Nutrient Pathways in a Temperate Headwater Catchment, Hydrological Processes, 38, e15308, https://doi.org/10.1002/hyp.15308, 2024.

Penna, D., Tromp-van Meerveld, H. J., Gobbi, A., Borga, M., and Dalla Fontana, G.: The influence of soil moisture on threshold runoff generation processes in an alpine headwater catchment, Hydrology and Earth System Sciences, 15, 689–702, https://doi.org/10.5194/hess-15-689-2011, 2011.

Rakovec, O., Samaniego, L., Hari, V., Markonis, Y., Moravec, V., Thober, S., Hanel, M., and Kumar, R.: The 2018-2020 Multi-Year Drought Sets a New Benchmark in Europe, Earth Future, 10, e2021EF002394, https://doi.org/10.1029/2021ef002394, 2022.

Singh, N. K., Emanuel, R. E., McGlynn, B. L., and Miniat, C. F.: Soil Moisture Responses to Rainfall: Implications for Runoff Generation, Water Resources Research, 57, e2020WR028827, https://doi.org/10.1029/2020wr028827, 2021.

Speir, S. L., Rose, L. A., Blaszczak, J. R., Kincaid, D. W., Fazekas, H. M., Webster, A. J., Wolford, M. A., Shogren, A. J., and Wymore, A. S.: Catchment concentration-discharge relationships across temporal scales: A review, Wiley Interdisciplinary Reviews-Water, 11, e1702, https://doi.org/10.1002/wat2.1702, 2024.

Stewart, B., Shanley, J. B., Kirchner, J. W., Norris, D., Adler, T., Bristol, C., Harpold, A. A., Perdrial, J. N., Rizzo, D. M., Sterle, G., Underwood, K. L., Wen, H., and Li, L.: Streams as Mirrors: Reading Subsurface Water Chemistry From Stream Chemistry, Water Resources Research, 58, e2021WR029931, https://doi.org/10.1029/2021wr029931, 2022.

https://doi.org/10.5194/egusphere-2026-4221
Preprint. Discussion started: 17 July 2026
© Author(s) 2026. CC BY 4.0 License.

Tarasova, L., Basso, S., Zink, M., and Merz, R.: Exploring Controls on Rainfall-Runoff Events: 1. Time Series-Based Event Separation and Temporal Dynamics of Event Runoff Response in Germany. Water Resources Research, 54, 7711–7732, https://doi.org/10.1029/2018wr022587, 2018.

Tetzlaff, D., Soulsby, C., Buttle, J., Capell, R., Carey, S. K., Laudon, H., McDonnell, J., McGuire, K., Seibert, J., and Shanley, J.: Catchments on the cusp? Structural and functional change in northern ecohydrology, Hydrological Processes, 27, 766–774, https://doi.org/10.1002/hyp.9700, 2013.

Thiesen, S., Darscheid, P., and Ehret, U.: Identifying rainfall-runoff events in discharge time series: a data-driven method based on information theory, Hydrology and Earth System Sciences, 23, 1015–1034, https://doi.org/10.5194/hess-23-1015-2019, 2019.

Tromp-van Meerveld, H. J., and McDonnell, J. J.: Threshold relations in subsurface stormflow: 2, The fill and spill hypothesis, Water Resources Research, 42, W02411, https://doi.org/10.1029/2004wr003800, 2006.

Werner, B. J., Lechtenfeld, O. J., Musolff, A., de Rooij, G. H., Yang, J., Gründling, R., Werban, U., and Fleckenstein, J. H.: Small-scale topography explains patterns and dynamics of dissolved organic carbon exports from the riparian zone of a temperate, forested catchment, Hydrology and Earth System Sciences, 25, 6067–6086, https://doi.org/10.5194/hess-25-6067-2021, 2021.

Wollschläger, U., Attinger, S., Borchardt, D., Brauns, M., Cuntz, M., Dietrich, P., Fleckenstein, J. H., Friese, K., Friesen, J., Harpke, A., Hildebrandt, A., Jäckel, G., Kamjunke, N., Knöller, K., Kögler, S., Kolditz, O., Krieg, R., Kumar, R., Lausch, A., Liess, M., Marx, A., Merz, R., Mueller, C., Musolff, A., Norf, H., Oswald, S. E., Rebmann, C., Reinstorf, F., Rode, M., Rink, K., Rinke, K., Samaniego, L., Vieweg, M., Vogel, H. J., Weitere, M., Werban, U., Zink, M., and Zacharias, S.: The Bode hydrological observatory: a platform for integrated, interdisciplinary hydro-ecological research within the TERENO Harz/Central German Lowland Observatory, Environmental Earth Sciences, 76, 29, https://doi.org/10.1007/s12665-016-6327-5, 2017.

Zimmer, M. A., and McGlynn, B. L.: Lateral, Vertical, and Longitudinal Source Area Connectivity Drive Runoff and Carbon Export Across Watershed Scales, Water Resources Research, 54, 1576–1598, https://doi.org/10.1002/2017wr021718, 2018.

Zuecco, G., Penna, D., Borga, M., and van Meerveld, H. J.: A versatile index to characterize hysteresis between hydrological variables at the runoff event timescale, Hydrological Processes, 30, 1449–1466, https://doi.org/10.1002/hyp.10681, 2016.